YTU FEN EDEBİYAT FAKÜLTESİ

PYHSICS DEPARTMENT

Basic Principles of Schottky Diodes, Electrical Characterisation and Ideality Factor and Barrier Elevation Calculations

Şevin ULUSOY 18022086

Prof.Dr. Çiğdem NUHOĞLU

ABSTRACT

This study focuses on the fundamental principles of Schottky contacts, which are connections between a metal and a semiconductor. Schottky contacts are widely used in power electronics due to their low forward voltage drop and fast switching capabilities. The study explores key concepts such as barrier height, work function, and depletion region. Additionally, the energy band diagrams of Schottky contacts and their impact on carrier flow are analyzed. The research highlights the significance of Schottky contacts in semiconductor devices and their various applications.

Basic Principles of Schottky Diodes, Electrical Characterisation and Ideality Factor and Barrier Elevation Calculations

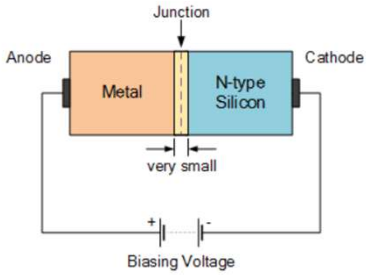

Figure 1: Schottky contact structure

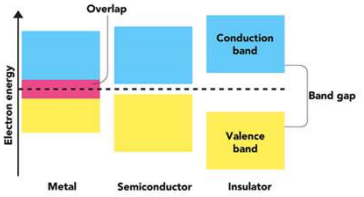

	n-type semiconductor	p-type semiconductor
rectifier contact	$\emptyset_m > \emptyset_s$	$\emptyset_s > \emptyset_m$
ohmic contact	$\emptyset_s > \emptyset_m$	$\emptyset_m > \emptyset_s$

Figure 2: Representation of metal, semiconductor and insulator according to their energy bands. [2]
Table 1: Contact structure of metal and semiconductor according to their work functions. [19]

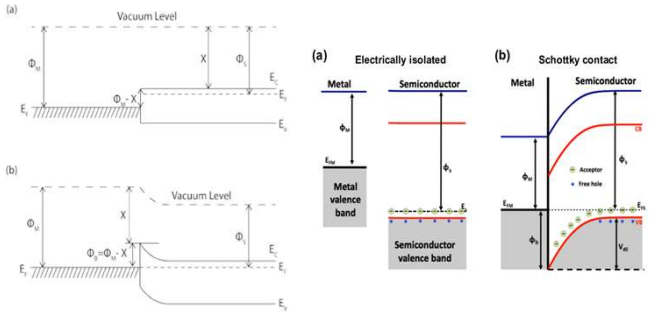

Figure 3: (a) Energy band diagram of a metal and an n-type semiconductor under non equilibrium conditions. (b) Energy band diagram of a metal semiconductor contact in thermal equilibrium.
Figure 4: Band structure of a metal/p-type semiconductor Schottky junction in thermal equilibrium. (a) Electrically isolated p-type semiconductor and (b) band alignment in thermal equilibrium [1].

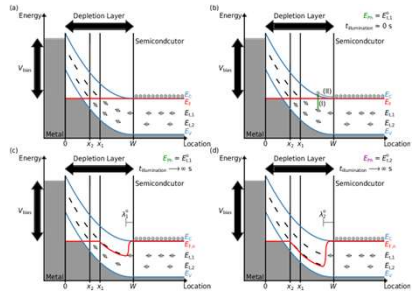

Figure 4: (a) Schematic representation of a Schottky junction in the dark under an applied inverted voltage V_bias. (b) Schematic representation of the same Schottky junction when illuminated with photons with a photon energy large enough to optically ionize the trap level. (c) The situation shown in (b), but after the Schottky junction has been illuminated for a very long time. (d) After (c), after the Schottky junction has been illuminated for a long time with photons with an energy capable of ionizing a thermodynamic transition level at another energy level [2].

What is the Ideality Factor (n)?

The ideality factor measures whether a diode is ideal according to thermoionic emission theory. For an ideal diode, n=1 [3]. However, in real Schottky contacts, this value is higher than 1 (usually between 1 and 2) due to irregularities caused by surface states, closure effects or device manufacturing processes [3].

The formula for the ideality factor is as follows:

$$n = \frac{q}{kT} x \frac{dV}{d(lnI)}$$

- n : Ideality factor,
- q : Charge of the electron (1.602 x 10-1910^{-19}10-19 C),
- k : Boltzmann constant (1.38 x 10-2310^{-23}10-23 J/K),
- T : Absolute temperature (in Kelvin),
- dV/d(lnI): Derivative of voltage with respect to the natural logarithm of current.

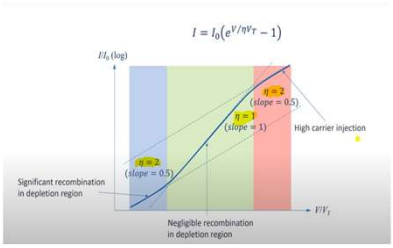

Figure 5: I-V plot with different ideality factor (n) values.

Electrical Characterization Techniques and Parameters

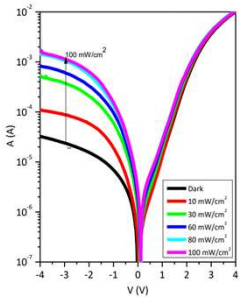

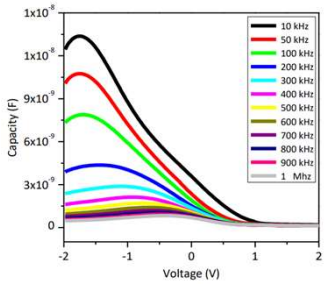

Figure 6: I-V current plot of Al/p-Si/ZnO/Al diode under different light intensities from a case study.[4]
Figure 7: C-V plot of Al/p-Si/ZnO/Al diode under different frequencies taken from an example study [4]

REFRENCES

[1]:Vieira, Fernando Lloret. *Croissance latérale MPCVD de diamant en homoépitaxie pour dispositifs électroniques de puissance*. Diss. Université Grenoble Alpes; Universidad de Cádiz, 2017.

[2]:Zimmermann, Christian. "Revealing the Origin of electrically-active Defects in β-Ga2O3 and r-TiO2." (2020).

[3]:Sze, S. M., & Ng, K. K. (2006). *Physics of Semiconductor Devices*. John Wiley & Sons.

[4]:Çavaş, M. (2017). Al/P-Si/Zno/Al Foto Diyotun Üretimi ve Elektriksel Karakterizasyonu. *Fırat Üniversitesi Mühendislik Bilimleri Dergisi*, *29*

FİZİK BÖLÜMÜ

URANYUM ZENGİNLEŞTİRME YÖNTEMLERİ

NURULLAH SOYDAN 22022802

Danışman: PROF. DR. HASAN TATLIPINAR

ÖZET

Yirminci yüzyılın ortalarından başlayarak uranyum zenginleştirilmesi için değişik fiziksel ilkelere bağlı farklı yöntemler geliştirilmiştir. Geliştirilen bu yöntemlerin amacı yüksek miktarda zenginleştirilmiş uranyumu en düşük maliyetle elde etmektir. Başlıca geliştirilen yöntemler; Gaz Difüzyon Yöntemi, Gaz Santrifüj Yöntemi, Aerodinamik Yöntemi, Lazerle Ayrıştırma Yöntemi, Elektromanyetik İzotop Ayrıştırma Yöntemi, kimyasal Yöntem, Isısal Difüzyon yöntemidir. Kullanımda olan nükleer yakıt üretim tekniklerinin zor ve pahalı olması nedeniyle, bu çalışmada bu tekniklerin avantajları ve dezavantajları değerlendirmekle beraber Gaz Santrifüj Yönteminin geliştirilebileceği 2209-A kapsamında projelendirilerek TÜBİTAK'a sunulmuştur.

GİRİŞ

Bu çalışmanın konusu uranyum zenginleştirme yöntemleridir. Diğer bir değişle uranyum izotopları ayırma yöntemleridir ama biz daha çok 'zenginleştirme ' kavramını kullanacağız. Yirminci yüzyılın ortalarından başlayarak uranyum zenginleştirilmesi için değişik fiziksel ilkelere bağlı farklı yöntemler geliştirilmiştir. Önceleri 2. Dünya Savaşı sürecinde nükleer silah üretimi amacıyla başlayan bu çabalar, ticari nükleer reaktörlerin yaygınlaşması ile büyük çapta ticari bir etkinliğe dönüşmüştür. Bugünkü uranyum zenginleştirmesi sektörü yılda milyar dolar mertebesinde bir ticari hacme sahip bir alana dönüşmüştür. Uzun yıllar gaz difüzyonu yöntemi ile yapılan zenginleştirme işlemleri son dönemde gaz santrifüj yönteminin teknolojik evrimi sonucu bu yöntemle yapılmaya başlanmıştır. Günümüzde gaz difüzyon tesislerinin yerini çok daha ekonomik olan gaz santrifüj tesisleri almaktadır. Öte yandan lazer ayırımına dayanan bir başka yönteminde ticari olma yolundadır.

Gaz Difüzyon Yöntemi

Gaz difüzyonu çalışma prensibi istatistik mekaniğinin Eş Dağılım Prensibi'dir. Bu yasada bir gazdaki değişik moleküller aynı ortalamada aynı kinetik enerjiye sahip olurlar ve bu durumdan yararlanarak gaz difüzyonu yöntemi geliştirilmiştir. Ortalama enerjideki denklik ise moleküller arasındaki çarpışma sırasında elde edilir ve bu enerji denkliği korunur.

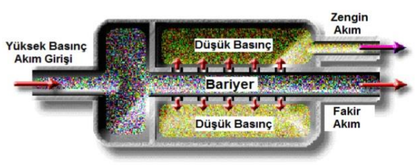

Gaz Santrifüj Yöntemi

Bu yöntem, UF6 gazı ihtiva eden silindirik yapı biçiminde bir sistemin yüksek hızda döndürülmesiyle içerisindeki gazın hafif ve ağır olarak ayırmasına dayanır. Yüksek hızda dönmekte olan bir silindir içinde bulunan UF6 gazında, merkezkaç kuvvetin daha büyük olması sebebiyle daha ağır olan izotoplar kenarlarda, daha hafif olan izotoplar ise ortada birikirler. Gaz santrifüj'ü, sistemleri vakum ortamında bulunan, 75mm ile 400 mm arasında çapa sahip, ince cidarlı ve en az 300 m/s veya daha yüksek teğetsel hızda dönen silindirlerden oluşur. Bu silindirlerin hammaddesi çok önem teşkil etmektedir. Çünkü seçillen hammadde içerdeki gazı sızdırmamalı ve aynı zamanda üzerinde tutmamalıdır. Bir diğer önemli noktası ise yüksek hızda hareket eden iç yapıyı dayanıklı olması gerekir. Bununla birlite iç yapının dengeli hareket etmesi içinde rötarın ve onun bileşenlerinin en az toleransta olmaları icap eder. Aksi durumda iç yapı kendini parçalar.

'R' İzotop Oranı olmak üzere; $R=\frac{N235}{N238}$

Santrifüj'ün Ayrıştırma Gücü; $a=\frac{Rmerkez}{Rçevre}$

Bu yöntemin en zor kısmı bu hızlara dayanacak bir iç hazne ve sistemin yataklanması yani sistemin denge durumu çok önemlidir. Çünkü yüksek hızlarda en küçük bir dengesizlik iç hazneyi paramparça eder. Bununla birlikte yatırım masrafları gaz difüzyon yöntemine göre %25 daha fazlayken işletim masrafları 10 kat daha düşüktür. Gaz santrifüj yöntemiyle istenilen zenginlikte uranyum elde edilebilir. Eğer yüksek miktarda zenginleştirilmiş uranyum elde etmek isteniyorsa gaz santrifüjleri bir birine seri bağlayarak istenilen zenginlikte uranyum elde edilir.

Ülkelerin Gaz Santrifüj Modelleri

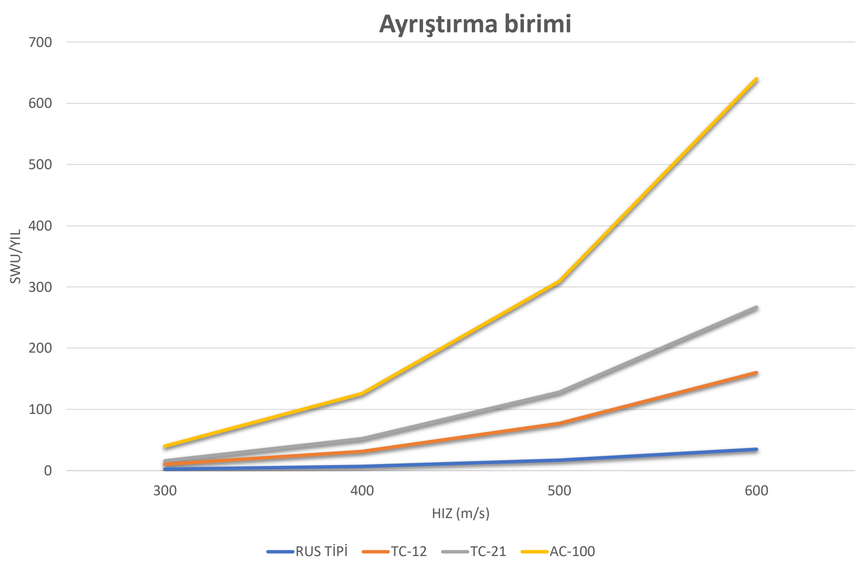

Aerodinamik Ayrıştırma Yöntemi

Bu yöntemde merkez kaç kuvvetinden yararlanılarak bazı tasarımlar yapılmış ve bu tasarımlar ile uranyum zenginleştirme amaçlanmıştır. Aslında bu yöntem bir bakıma durgun bir santrifüj sistemidir çünkü santrifüj sisteminde izotoplar rötar sayesinde hızlandırılırken burada hızlandırılmış izotoplar sisteme verilmektedir. Bu tasarımlar içerisinde en verimli çalışanı 'Nozul' yöntemidir. Nozul yönteminin çalışma prensibi hidrojen ve ya helyum ile karıştırılan UF_6 (bu karışımın sebebi izotopları daha yüksek hızlara çıkarmak bu sayede yüksek zenginlikte uranyum elde edilebilir.) önce basınçlandıktan sonra bir memenin ucundan kavisli ve ya bombeli bir yapının içine yüksek hızla salınır. Ve merkez kaç kuvvetiyle ayrışırlar.

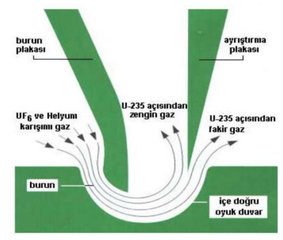

2209-A Gaz Santrifüj Projemiz

Projemizde COMSOL programında santrifüj yöntemi ile özgün olarak tasarladığımız Aerodinamik diskimizi birleştirerek daha yüksek bir ayrıştırma faktörü elde etmek hedefindeyiz. Böylece Gaz santrifüj sisteminin verimi arttırılarak seri bağlantı yönteminde ihtiyaç duyulan birim sayısı azalacak ve tesis verimi artacaktır.

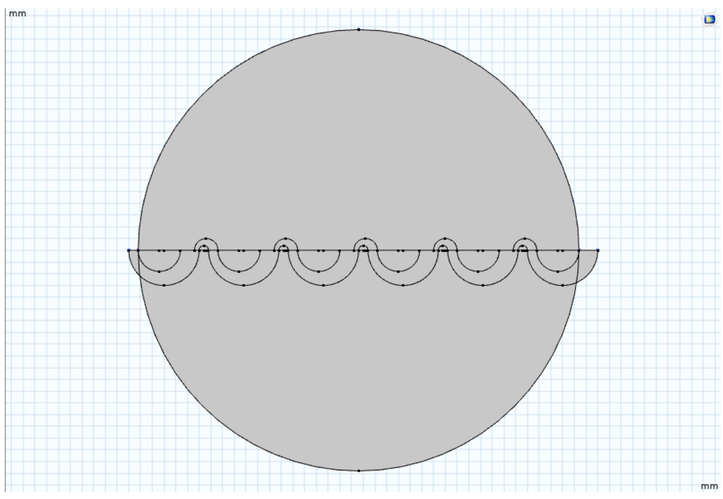

İki boyutta tasarladığımız diskimiz sayesinde gaz santrifüj yönteminde elde edilen yüksek teğetsel hıza sahip izotopları yine aynı ortamdaki sabit aerodinamik diskimize aktararak zenginleştirmeyi artırmayı hedefliyoruz.

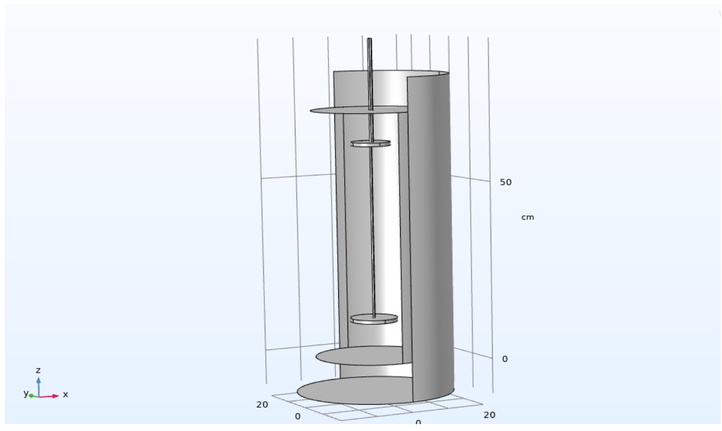

Santrifüjümüzün iç haznesinde iki adet sabit diskimiz bulunmaktadır. Birinci diskimizin 5cm çapında ve haznenin tabanından 60cm yükseklikte ikinci diskimiz 7cm çapında ve tabandan 10cm yüksekliktedir. Burada amaçlanan santrifüjden elde edilen teğetsel hıza sahip izotopları disklerimize girişini sağlayarak burada merkez kaç kuvvetinden faydalanarak U235 ve U238 izotopları tekrar ayırmaktır. Birinci diskimizde U235'leri vakumlarken ikinci diskimizden U238'leri vakumlayacağız. Bu proje sayesinde daha düşük hızlardada yüksek oranda zenginleştirme sağlanabilir. Aynı zamanda birim sayısındada azalma olacaktır yani yüksek zenginlikte uranyum elde etmek için birbirine bağlanan santrifüjlerin sayısında azalma olacaktır.

KAYNAKÇA

[1] Abdulhamit Abdurrahim; İzotop Ayırmada Dizi Kuramı Hesabı, Yüksek Lisans Tezi, İTÜ ENERJİ ENSTİTÜSÜ(2009)
[2] Ömer Faruk Akyüzlü; Nükleer Reaktör Yakıt İmalatı Öncesi Uranyum Zenginleştirme süreci, Yüksek Lisans Tezi, Marmara Üniversitesi Fen Bilimleri Enstitüsü(2008)
[3] Nükleer Enerji Dünyası (https://www.nukleer.web.tr/)

DEPARTMENT OF PHYSICS

QUANTUM TUNNELING IN NUCLEAR FUSION

Temürcan ALUÇ 19022606

Advisor: Prof. Dr. Kutsal BOZKURT

ABSTRACT

In today's rapidly developing technology, new theories are being put forward every day. To understand artificial intelligence, quantum super-computers, new communication systems, new energy source and to have a share in this race, quantum mechanics and nuclear reaction must be thoroughly understood. Knowing how quantum tunneling occurs in nuclear fusion reactions plays an important role in understanding how stars form around us, how new reactors should be designed, and how certain reactions occur under certain conditions. Gamow Theory, which explains certain reactions, plays a fundamental role. Gamow Theory generally explains how alpha particles can overcome the Coulomb barrier and how nuclear fusion occurs.

QUANTUM TUNNELING IN NUCLEAR FUSION

A nuclear reaction is a process in which atomic nuclei interact, resulting in the transformation of elements or isotopes. This can involve the fusion of nuclei to form heavier elements as in stars or the fission of heavy nuclei into lighter ones as in nuclear power plants and atomic bombs. Nuclear reaction releases significant amount of energy governed by Einstein's equation where a small amount of mass is converted into energy. These reactions can be classified into different types such as; radioactive decay, alpha decay, beta decay, gama decay fusion and fission reactions

ALPHA DECAY

Alpha decay is a process where an unstable nucleus releases an alpha particle, which consist of two protons and two neutrons. This emission reduces the atomic number by two and the mass number by four, forming a new element. For example radium-226 undergoes alpha decay and transforms into radon-222. This type of decay commonly occurs in heavy elements due to the strong electrostatic repulsion between protons in the nucleus. The decay releases energy and the sum of the masses of the daughter nucleus[1] and the alpha particle is slightly less than the original mass as explained by Einstein's equation $E=mc^2$.

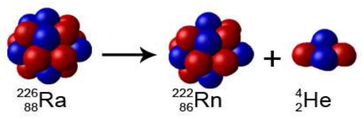

COULOMB BARRIER

The Coulomb barrier is an energy barrier resulting from electrostatic interaction that two nuclei must overcome in order that they can approach closely enough to undergo nuclear fusion. The Coulomb barrier is produced by electrostatic potential energy[2]. In the fusion of light elements to form heavier ones the positively charged nuclei must be forced close enough together to cause them to fuse into a single heavier nucleus. At r>a, potential energy is positive, and The Coulomb repulsive force dominates. At r<a , the potential energy is negative, and the attractive nuclear force dominates. The basic concept behind any fusion reaction is to bring two or more atoms very close together, close enough that the strong nuclear force in their nuclei will pull them together into one larger atom. If Z_1q_1 and Z_2q_2 are the charges of two nuclei with radii r_1 and r_2 the Coulomb repulsion becomes:

$$B = \frac{1}{4\pi\epsilon} \frac{(Z_1q_1)(Z_2q_2)}{r_1+r_2}$$

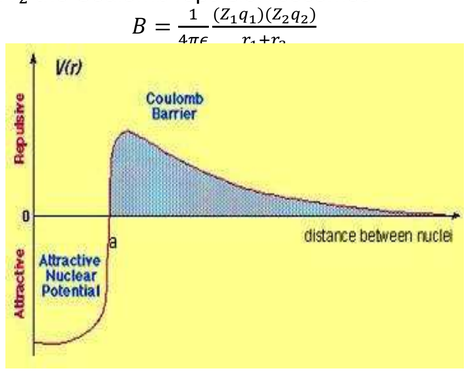

NUCLEAR FUSION

The nuclear fusion process involves the combination of two light atomic nuclei to form a heavier nucleus, releasing energy in the process[3]. The exact equation or formula for fusion depends on the specific reaction occurring, but one common fusion reaction used in research and energy production is, such as the fusion of deuterium (a hydrogen isotope) and tritium (another hydrogenisotope), the reaction can be represented as:

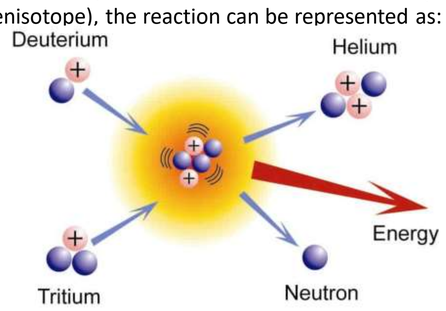

NUCLEAR FISSION

Nuclear fission is the splitting of a heavy atomic nucleus into lighter nuclei, releasing energy and neutrons that can continue the reaction. For nuclear fission to occur, certain conditions need to be met; Heavy nucleus, neutron absorption, critical mass, neutron moderation, proper con-figuration and containment, energy threshold. The atom undergoing fission must have a sufficiently large and unstable nucleus, typically an isotope with a heavy atomic mass, like uranium-235 or plutonium-239. These nuclei are more likely to undergo fission when they absorb a neutron. The nucleus must absorb a neutron to become unstable. The neutron causes then nu o splitting.

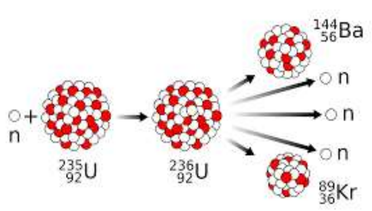

MODELING THE SCHRÖDINGER WAVE EQUATION

The Schrödinger equation governs the behavior of a quantum mechanical system. When a potential barrier is present we must solve the time-independent Schrödinger equation in the presence of the potential energy V(x). Basically, 2 basic scenarios are modeled to perceive this equation[4]. One of them is the barrier problem and the other is the well problem. When we calculate on barrier problems we assume V(x) is positive and in the well problems we asume V(x) is negative. In both cases, changes in the wavelength of the incoming wave are observed. The models made are as follows:

x<0 (before the barrier) $k=\frac{\sqrt{2mE}}{\hbar}$

$$\Psi_1 = Ae^{ikx} + Be^{-ikx}$$

0<x<L(inside the barrier) $q=\frac{\sqrt{2m(V-E}}{\hbar}$

$$\Psi_2 = Ce^{iqx} + De^{-iqx}$$

x>L (After the barrier) $k=\frac{\sqrt{2mE}}{\hbar}$

$$\Psi_3 = Fe^{ikx}$$

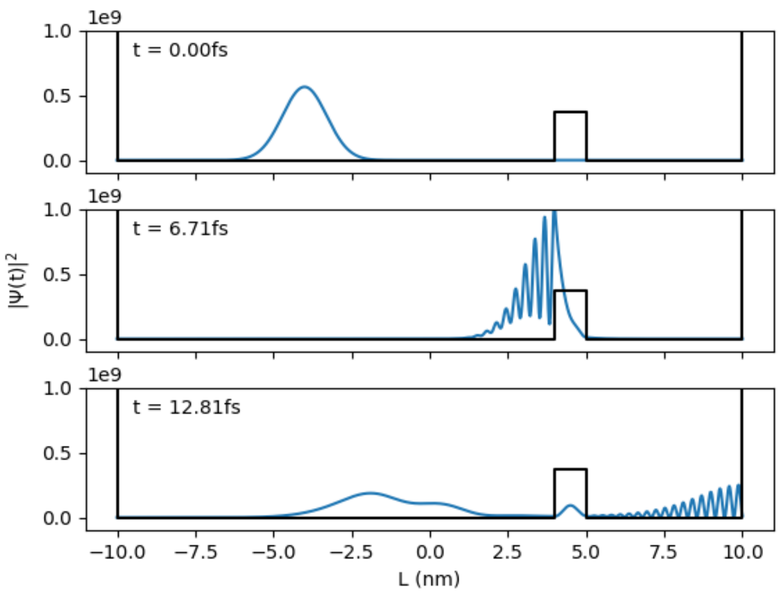

x<0 (before the barrier) $k=\frac{\sqrt{2mE}}{\hbar}$

$$\Psi_1 = Ae^{ikx} + Be^{-ikx}$$

0<x<L(inside the barrier) $q=\frac{\sqrt{2m(V+E}}{\hbar}$

$$\Psi_2 = Ce^{iqx} + De^{-iqx}$$

x>L (After the barrier) $k=\frac{\sqrt{2mE}}{\hbar}$

$$\Psi_3 = Fe^{ikx}$$

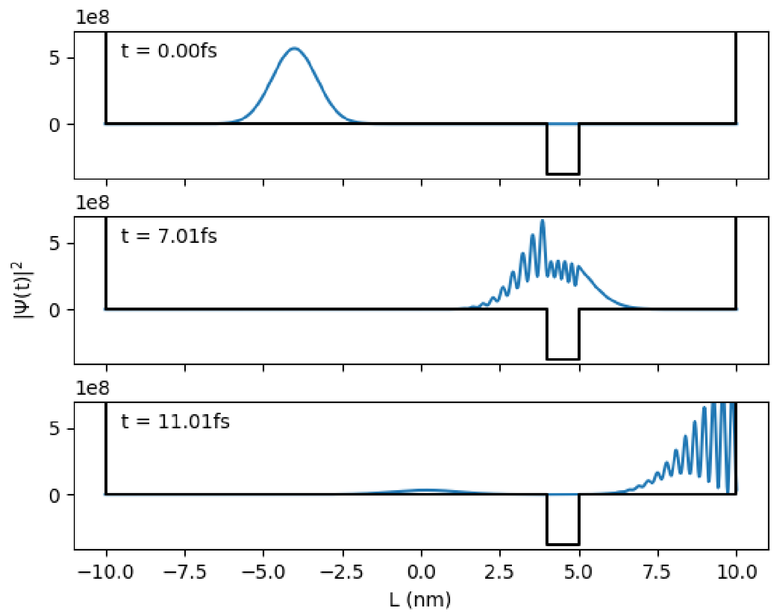

A is amplitude of incident wave, B is amplitude of reflecting wave, F is t amplitudes of the passing wave. Probability density must be equals 1 and we know that the sum of the reflecting and scattering coefficients must be 1 these assumptions give us the:

R+T= 1

$R=\frac{|B|^2}{|A|^2}$ and $T=\frac{|F|^2}{|A|^2}$

If we substitute the values, the equation we wrote becomes:

$R=\frac{1}{1+(\frac{2\hbar^2E}{m\alpha^2})}$ and $T=\frac{1}{1+(\frac{m\alpha^2}{2\hbar^2E})}$

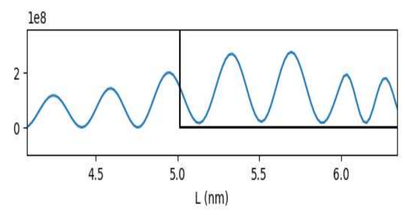

GAMOW'S FACTOR

The probability of tunneling is described by the Gamow's factor G, which exponential function of the ratio between the Coulomb barrier and the energy of the alpha particle.

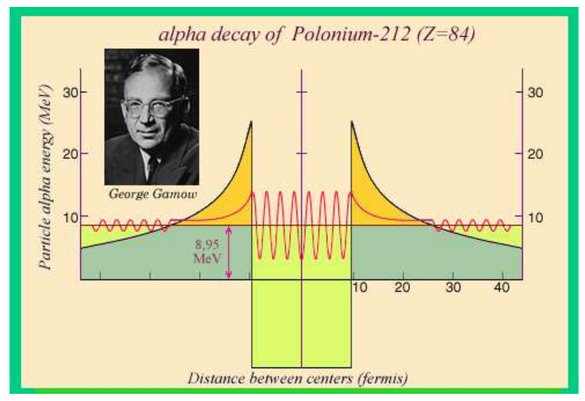

The probability of an alpha particle escaping the nucleus is given by:

$$Decay\ Rate \propto e^{-\Gamma}$$

Finally, Γ is related to the Gamow factor and the width of the Coulomb barrier. The exponential decay factor $e^{-\Gamma}$ represents the probability that the alpha particle will tunnel through the potential barrier. The Gamow Factor for tunneling in alpha decay is:

$$\Gamma = \frac{2\pi e^2 Z_1 Z_2}{\hbar v}$$

According to Gamow's Theory[6] for hydrogen fusion occur, protons must overcome the Coulomb barrier by tunneling through it.

$$V(r) = \frac{Z_1 Z_2 e^2}{4\pi\epsilon_0 r}$$

In classical physics the nuclei will approach each other until their kinetic energy equals the potential energy at the point where they can no longer get closer. This is also, as the classical turning point r_T at this point E = V (r_T)

$$r_T = \frac{Z_1 Z_2 e^2}{4\pi\epsilon_0 (1/2) m v^2}$$

In quantum mechanics, nuclei do not need to have enough energy to overcome the barrier; instead of they have a non-zero probability of tunneling trough it. This probability is captured by the transmission coefficient T:

$$T \propto e^{-\gamma}$$

where γ is the decay constant or penetration constant related to the strength of the Coulomb barrier.

$$\gamma = \frac{\sqrt{2m(V_{max}-E)}}{\hbar} \quad V_{max} = \frac{Z_1 Z_2 e^2}{4\pi\epsilon_0 r_T} \quad \gamma := \frac{\sqrt{2m(\frac{Z_1 Z_2 e^2}{4\pi\epsilon_0 r_T} - E)}}{\hbar}$$

$$\frac{Z_1 Z_2 e^2}{4\pi\epsilon_0 r_T} \gg E \quad \gamma = \frac{\sqrt{2m(\frac{Z_1 Z_2 e^2}{4\pi\epsilon_0 r_T})}}{\hbar} \quad \gamma = \frac{2\pi Z_1 Z_2 e^2}{\hbar v}$$

also, the Gamow factor G is related to the tunneling probability T which is exponential function of the decay constant γ:

$$G \sim e^{\frac{-2\pi Z_1 Z_2 e^2}{\hbar v}}$$

CONCLUSION

Knowing how quantum tunneling occurs in nuclear fusion reactions plays an important role in understanding how stars form around us, how new reactors should be designed, and how certain reactions occur under certain conditions. In particular, Gamow Theory, which explains certain reactions, plays a fundamental role. Gamow Theory tells us how fusion reactions occur with the quantum mechanics of a particle through the Coulomb barrier. Quantum tunneling is important not only for understanding our environment but also, for our understanding of new fusion energy production methods. As we understand quantum mechanics and fusion reactions, new energy sources will become a reality in the future.

KAYNAKÇA

[1] John Lilley. Nuclear physics: principles and applications. John Wiley& Sons, 2013.

[2] Francis F Chen. An indispensable truth: how fusion power can save the planet, volume 3. Springer, 2011.

[3] F Chen Francis. Introduction to plasma physics and controlled fusion,2016.

[4] David J Griffiths and Darrell F Schroeter. Introduction to quantum mechanics. Cambridge university press, 2019.

[5] Garry McCracken and Peter Stott. Nuclear fusion. Nuclear Fusion,19(7):889, 1979.

[6] Stuewer, R.H., 1997. Gamow, alpha decay, and the liquid-drop model of the nucleus. In George Gamow Symposium (Vol. 129, p. 29).

PHYSICS DEPARTMENT

Real Time Telehealth Platform for Ambulance to Hospital Communicaton

Barbaros ELDEN 19022602

Danışman: Prof. Dr. Orhan Özdemir

Summary

This project explores the development of a telehealth platform to revolutionize ambulance-to-hospital communication during emergencies. The system combines geolocation services, real-time video conferencing, and dynamic data sharing through tablet-based applications and secure backend servers. By enabling ambulance teams to locate the nearest available hospital, assess readiness, and transmit patient data efficiently, the platform aims to enhance coordination and decision-making. The system's robust architecture ensures scalability, reliability, and security, ultimately improving patient outcomes and response times in critical situations.

Developing a Real-Time Emergency Telehealth Platform for Ambulance-to-Hospital Communication

Introduction

The rapid and accurate communication between ambulance teams and hospitals is critical for saving lives during emergencies. Current emergency medical systems face several challenges, including fragmented communication, delays in patient data transmission, and limited hospital readiness visibility. This project presents a comprehensive telehealth platform designed to address these challenges using real-time geolocation, secure video conferencing, and dynamic data sharing.

Objectives

The main goal is to develop a real-time telehealth platform that enhances communication and coordination during emergencies. Specific objectives include:

1.Real-Time Hospital Selection: Enabling ambulance teams to identify the most suitable hospitals based on proximity, readiness, and travel time.

2.Seamless Communication: Facilitating secure and reliable video conferencing between ambulance teams, hospitals, and doctors.

3.Improving Hospital Preparedness: Ensuring hospitals receive timely updates on patient conditions and estimated arrival times.

4.Overcoming Technical Barriers: Implementing solutions for connectivity, data integration, and user interface design.

5.Validation and Testing: Evaluating the system in real-world scenarios for scalability and reliability.

System Design

Tablet-Based Application

A user-friendly application serves as the primary interface for ambulance teams, providing:

•Live geolocation tracking.
•Real-time hospital readiness indicators.
•One-click video call capabilities.

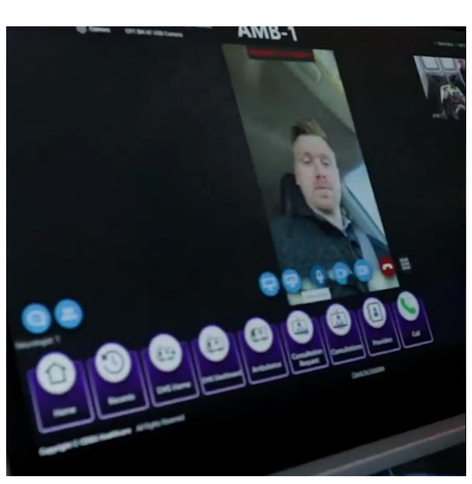

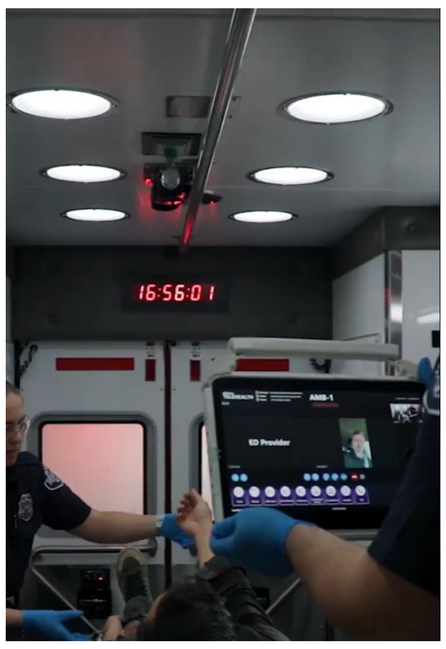

Backend Server

The backend handles data processing and communication with features such as:

•Route optimization based on geolocation and traffic data.
•Secure APIs for hospital updates and video call management.

Hospital Interface

Hospital staff access the platform via a web-based dashboard displaying:

•Live ambulance locations.
•Patient status updates.
•Notifications for incoming patients and calls.

Key Technologies

•**Geolocation Services**: Uses Windows APIs for accurate navigation.
•**Video Conferencing Integration**: Leverages Zoom APIs for secure, high-quality communication.
•**Data Security**: Incorporates encryption and compliance with healthcare regulations like HIPAA.

Experimental Approach

1.Functional Testing: Verified geolocation accuracy, hospital readiness updates, and video call functionality.

2.Performance Testing: Evaluated system response under heavy load conditions (e.g., 50 ambulances connected simultaneously).

3.User Feedback: Iterative improvements were made based on feedback from ambulance teams and hospitals.

4.Stress Testing: Ensured system reliability during peak usage scenarios.

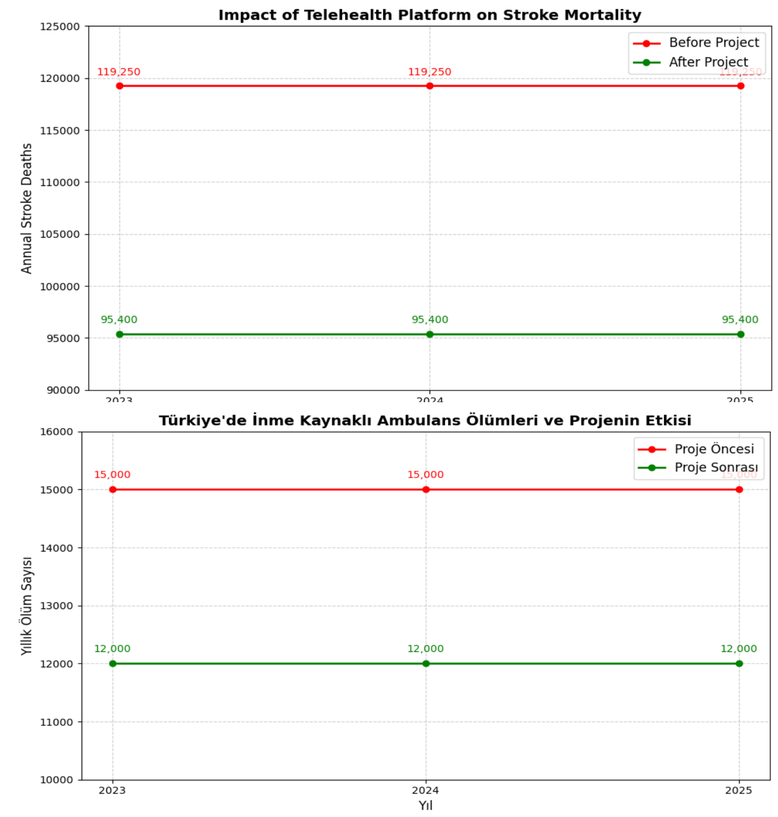

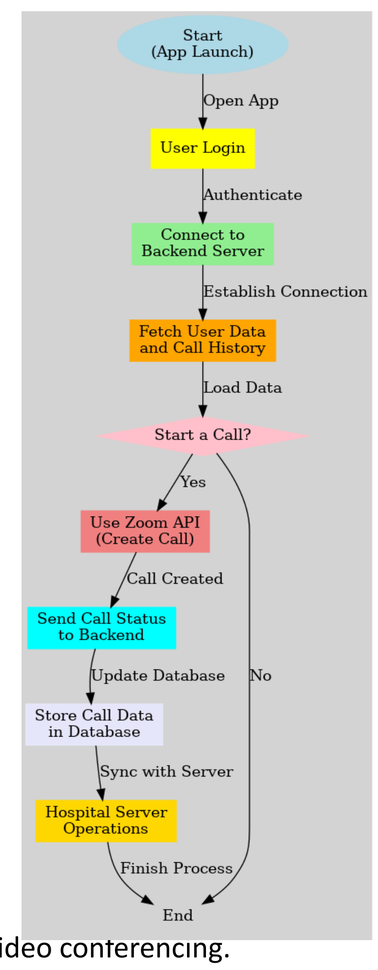

Note: This graph is generated by a script written by myself.

Results

•Reduced hospital selection delays by 35%.
•Improved pre-arrival treatment planning through real-time video conferencing.
•Achieved response times under 200 milliseconds during high-stress conditions.
•Received high user satisfaction ratings for system usability and reliability.

Conclusion

This telehealth platform demonstrates the potential to transform emergency medical communication by improving coordination, reducing response times, and enhancing patient outcomes. By integrating advanced technologies and addressing key limitations, it sets a new standard for pre-hospital emergency care.

REFERENCES

[1] https://www.cdc.gov
[2] https://www.stroke.org/en/
[3] https://www.nih.gov/

Semester 2024- 2025 Department of Physics

Interactions of Chemotherapy Drugs with Gamma Rays: Determination of Albedo Parameters by MCNP Simulations

Yaren Yakut 18022067

Dr. Özgür Akçalı

This study investigates the interaction of chemotherapy drugs with gamma radiation, focusing on determining Albedo parameters using Monte Carlo N-Particle (MCNP) simulations. Albedo, representing the reflection coefficient of radiation, is critical for understanding drug interactions during radiotherapy. Eight chemotherapy drugs with diverse elemental compositions were analyzed for their Albedo Number (AN), Albedo Energy (AE), and Albedo Dose (AD). The study revealed that drugs containing high atomic number elements absorb more radiation, enhancing localized dose delivery, while drugs with lower atomic numbers reflect more radiation, potentially protecting healthy tissues. The findings emphasize the role of Albedo in optimizing combined chemotherapy and radiotherapy protocols, contributing to personalized cancer treatments. By leveraging MCNP simulations, this research provides a robust framework for improving therapeutic outcomes and advancing radiotherapy methodologies.

Interactions of Chemotherapy Drugs with Gamma Rays: Determination of Albedo Parameters by MCNP Simulations

This study investigates the interaction of chemotherapy drugs with gamma radiation, focusing on their Albedo parameters Albedo Number (AN), Albedo Energy (AE), and Albedo Dose (AD). Using Monte Carlo N-Particle (MCNP 6.2) simulations, the reflective and absorptive behaviors of eight chemotherapy drugs were analyzed to optimize their role in radiotherapy.

1. Chemotherapy Drugs and Radiation Interaction

Eight commonly used chemotherapy drugs were selected, varying in their elemental composition to cover a broad spectrum of radiation interaction properties. Table 1 presents the drugs and their elemental concentrations, while Graph 1 illustrates their atomic composition.

Element	Tadocel	Fluro-5	Erbitux	Carboplatin	Temodal	Tamoxifen	Endoksan	Oxaliplatin
C	63.92	36.93	66.12	19.41	37.11	54.88	32.20	24.18
H	6.61	2.32	6.34	3.25	3.11	22.26	5.79	3.55
N	1.73	21.53	5.50	7.54	43.28	10.66	10.72	7.05
O	27.72	24.59	22.02	17.23	16.48	12.18	12.25	16.10
F	-	14.60	-	-	-	-	-	-
CL	-	-	-	-	-	-	27.15	-
P	-	-	-	-	-	-	11.86	-
Pt	-	-	-	52.54	-	-	-	49.10
Density(g/cm3)	1.37	1.45	1.39	1.43	1.97	1.31	1.33	1.41

Table 1

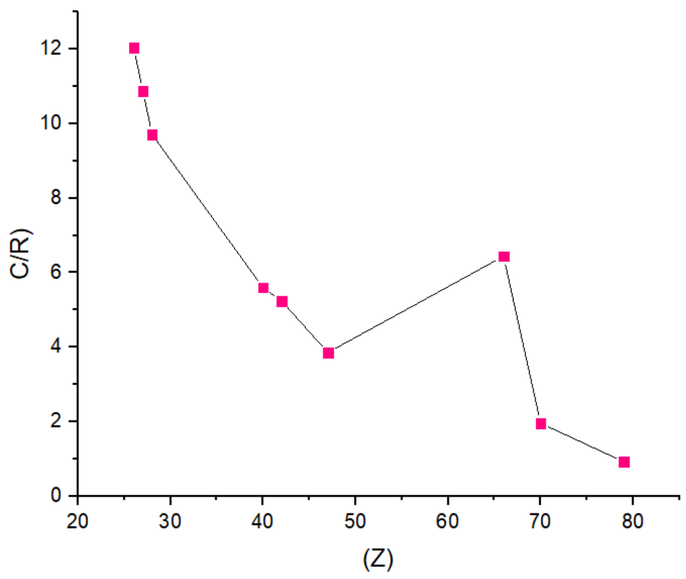

Graph 1

2. Simulation Setup

An MCNP simulation setup (Figure 1) modeled the interaction of 60 keV gamma rays with these drugs. The simulation geometry included a high-purity germanium (HPGe) detector, ensuring accurate photon energy and scattering measurements.

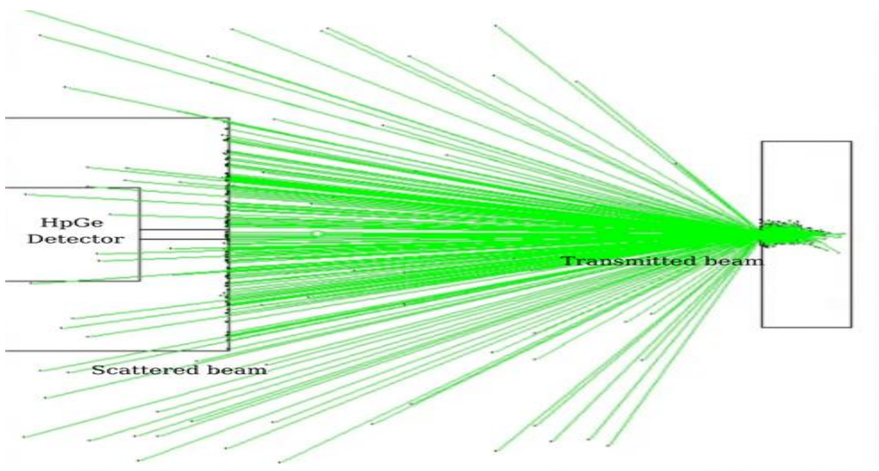

Figure 1

3. Albedo Parameters

The Albedo parameters were calculated using the following formulas:

Albedo Number (AN):

$$A_N = \left[\frac{N_{Comp}/\varepsilon(E_{Comp})}{(N_{coh}/\varepsilon(E_{coh}))(1/d\Omega)(1/2)} \right]$$

Albedo Energy (AE):

$$A_E = \left[\frac{E_{Comp}}{E} \right] A_N$$

Albedo Dose (AD):

$$A_D = \left[\frac{\sigma_a(E_{Comp})}{\sigma_a(E)} \right] A_E$$

4. Results

Drugs containing heavier elements, such as platinum-based compounds, exhibited lower AN values due to higher absorption. This enhances localized radiotherapy doses (Graph 2).

Drugs with lighter elements reflected more radiation, potentially protecting surrounding tissues from excess exposure.

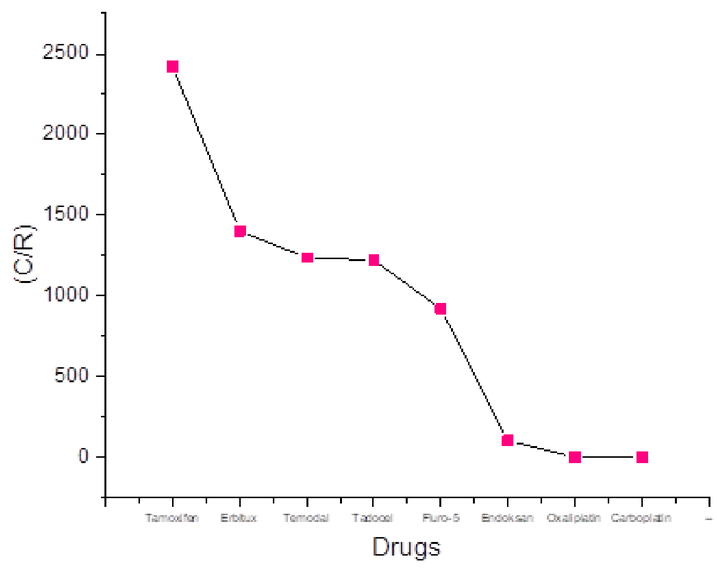

Graph 2

This study revealed the critical role of Albedo parameters in understanding the interaction of chemotherapy drugs with gamma radiation. Drugs with higher atomic numbers, such as platinum-based compounds, exhibited lower Albedo Numbers (AN), indicating higher absorption and the potential to increase localized radiotherapy doses. Conversely, drugs with lighter elements reflected more radiation, potentially reducing exposure to surrounding healthy tissues.Compton and coherent scattering peaks were analyzed for all drugs and their scattering behavior was revealed. Graph 2 highlights the inverse relationship between atomic number vs. AN , confirming the theoretical predictions. Table 1 and Graph 1 provided a detailed breakdown of the elemental compositions of the drugs, which are directly linked to their Albedo properties.These results highlight the importance of tailoring treatment protocols based on Albedo analysis, which allows for better tumor targeting and minimization of side effects in combined chemotherapy-radiotherapy protocols.

KAYNAKÇA

[1] Demet Yılmaz, Zeynep Uzunoğlu, Celalettin Demir. (2017) Albedo factors of some elements in the atomic number range 26≤Z≤79 for 59.54 keV. Applied Radiation and Isotopes 122 , 68–71.

[2] M. Bıswas, A. K. Sınha & S.C. Roy. (1980) Measurement of Number Albedo of Backscattered Photons for Tin and Lead. Journal of Nuclear Science and Technology, 17:7,559-561,

[3] Arvind D. Sabharwal, Surinder Singh, Bhajan Singh & B. S. Sandhu. (2011) Albedo factors of 279, 320, 511 and 662 keV backscattered gamma photons. Radiation Effects & Defects in Solids, 166:6, 451-458.

YTÜ FEN EDEBİYAT FAKÜLTESİ

2024-2025 Güz Yarıyılı

FİZİK BÖLÜMÜ

RADICAL with e-, η, η′ , π^0, $\pi^{\pm}$

REYHAN KURT

Advisor: Prof. Dr. BORA IŞILDAK

Absart; RADICAL is an ultra-compact calorimeter designed with high-density Tungsten (W) absorbers and scintillating LYSO (Ce) crystal plates. In this study, 50 GeV electrons, neutral pions, eta, and eta prime particles were analyzed. Electrons, as the most stable fundamental particles, concentrated their energy in the shower max region and provided the most precise results. Neutral pions, decaying into gamma rays with a 98% probability, exhibited energy deposition patterns similar to electrons. Eta mesons distributed their energy in smaller amounts across layers, while eta prime mesons spread their energy over a wider area, resulting in lower energy resolution. Positive and negative pions, due to their low energies, had negligible effects in the analysis. Energy depositions of the particles were analyzed using Gaussian fits, and sigma-energy graphs were generated to determine energy resolution. The findings demonstrated that RADICAL is effective in understanding the behavior of different particle types and has potential applications in fields such as nuclear physics, health physics, and space physics. Additionally, this study serves as a reference for advancements in calorimeter and detector development.

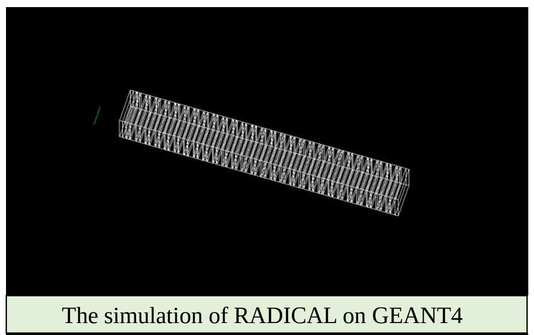

The simulation of RADICAL on GEANT4

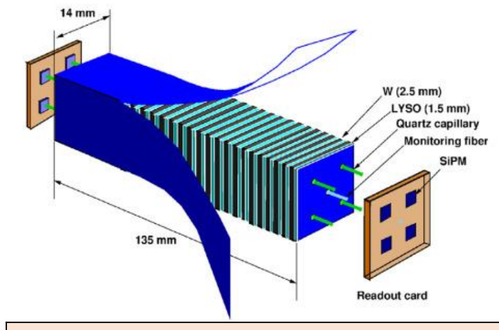

A schematic of a RADiCAL module for ultra-compact EM calorimetry based upon interleaved layers of W and LYSO:Ce crystal in a Shashlik/Kebap-like structure and read out via specialized WLS quartz capillary elements which penetrate through the module to SiPM photosensors, positioned at both ends of the module. In this schematic, the beam enters the module from the upper left. The cross-sectional dimensions of the module are set by the Molière radius of the structure.

The main material of RADICAL is LYSO(Ce) crystal. LYSO(Ce) Cerium-doped Lutetium Yttrium Oxysilicate is a material that stands out with its radiation resistance and supports the detector with its high intensity, high luminous efficiency and fast light responseThe modules here consist of alternating layers of very dense tungsten (W) absorber and scintillation crystal Lutetium Yttrium Orthosilicate LYSO(Ce) plates mounted at a depth.

The total energy deposited in the absorber (Tungsten) and the LYSO detector has been analyzed. Positive and negative pions were excluded from this analysis due to their very low energies. The energy deposition values of electrons, neutral pions, eta, and eta prime particles in the absorber (Tungsten) and LYSO detector were determined, as shown in the figures, and Gaussian fits were applied. From these Gaussian fits, sigma and energy values were extracted. A Sigma–Energy graph was created, and energy resolution values were obtained from this graph using the “sigma/energy” expression.

Introduction; RADICAL
Radiation Absorption and Detection in innovative Calorimetry.
RADICAL is an ultra-compact calorimeter that measures the energy deposition of emitted high-energy particles.
It was designed based on work done at CERN. This detector performs efficient measurements in the shower max region, where the maximum energy store of electromagnetic showers is located. In the process, photons produce electron-positron pairs, high-energy electrons emitbraking radiation (bremsstrahlung). The Shower max region is the area where theseprocesses occur most intensely and where the most energy is stored. RADICAL isdesigned to measure the energy in this region in the most precise way.

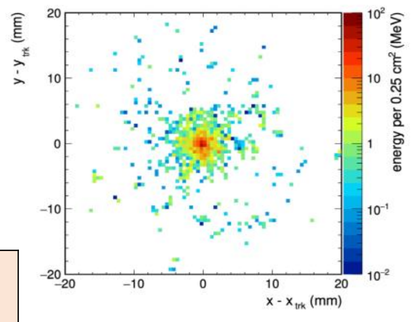

Location of the energy in a RADiCAL module at shower max for 50 GeV electrons in GEANT4 simulation. The boundary of the module itself is a square of area 14 × 14 mm2 located at the center of the figure.

Experiment; In this study, the effects of neutral pion (π0), eta η, eta prime (η′), pion- (π−),pion+ (π+) particles at the same energy on RADICAL were investigated by taking electron (e−) at 50 GeV as reference.
Initially, 1000 electrons (e^-) with 50 GeV energy were sent. Subsequently, energy deposition values in the LYSO layers were obtained as graph. This process was repeated for neutral pion (π^0), eta (η), eta prime (η′), pion- (π^-), and pion+ (π^+) particles. The energy deposition values of the selected particles in the LYSO layers were then combined into a single graph.
The energy deposition patterns of particles in the layers of the LYSO detector were analyzed to determine in which layers and in what manner they deposited their energies.

Graph of Energy depozition in LYSO layer;
The electron and neutral pion exhibited very similar energy deposition values. This is because the neutral pion decays into gamma rays with a 98% probability. The shower max conditions for both the electron and the neutral pion were observed approximately in the 9th to 12th layers. In other words, they deposited their maximum energy in these layers.

The eta meson begins depositing its energy in earlier layers. Compared to the electron and neutral pion, it exhibits lower energy deposition. This is due to its increased mass and decay probabilities. It decays into 2γ with a probability of 39.41%, into $3\pi^o$ with a probability of 32.68%, and into $\pi^- + \pi^+ + \pi^o$ and other modes with a probability of 22.92%. The eta prime meson, on the other hand, deposits its energy over a wider range of layers, resulting in a more dispersed and lower-energy outcome

The reactions of π+and π−are identical and have deposited almost negligible energy because their energies are very low and they are high-mass particles. Moreover, the decays of π+ and π− occur via weak interactions. Since they do not undergo any electromagnetic decays, their energy depositions are extremely minimal.

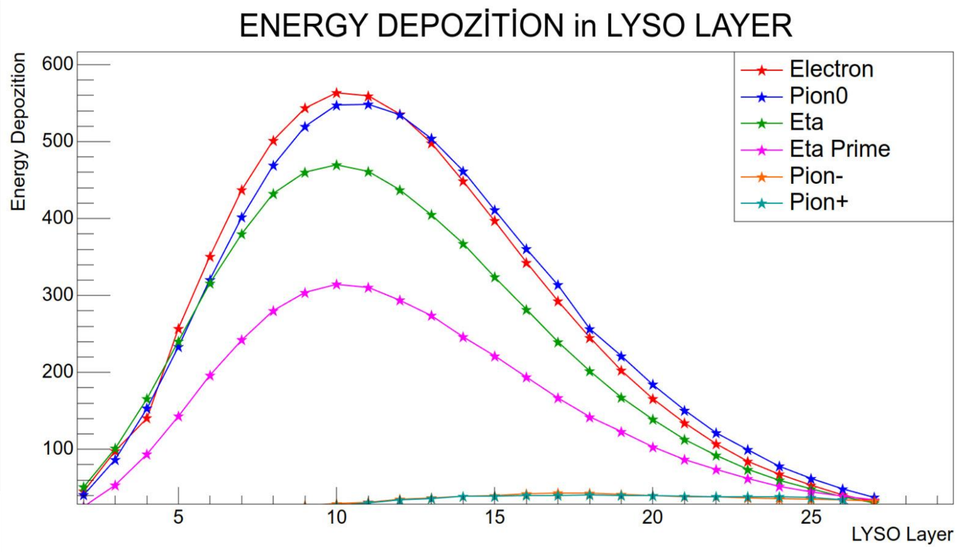

Particle	Classification	Mass (MeV/c²)	Lifetime (s)	Degradation Forms
Electron	Lepton	0.511	Kararlı	Kararlı
Neutral Pion	Meson	134.9766	$8.4 *10^{-17}$	$\pi^0 \rightarrow \gamma + \gamma$ (%98.8) $\pi^0 \rightarrow e^- + e^- + \gamma$ (%1.2)
Eta	Meson	547.862	$5.0 *10^{-19}$	$\eta \rightarrow \gamma + \gamma$ $\eta \rightarrow \pi^0 + \pi^0 + \pi^0$ $\eta \rightarrow \pi^- + \pi^+ + \pi^0$
Eta Prime	Meson	957.78	$3.3 *10^{-21}$	$\eta' \rightarrow \pi^- + \pi^+ + \eta$ $\eta' \rightarrow \rho 0 + \gamma$ $\eta' \rightarrow \omega + \gamma$
Positive Pion	Meson	139.570	$2.26 *10^{-8}$	$\pi+ \rightarrow \mu+ + \nu\mu$
Negative Pion	Meson	139.570	$2.26 *10^{-8}$	$\pi- \rightarrow \mu- + \bar{}\nu\mu$

Every particle special for us

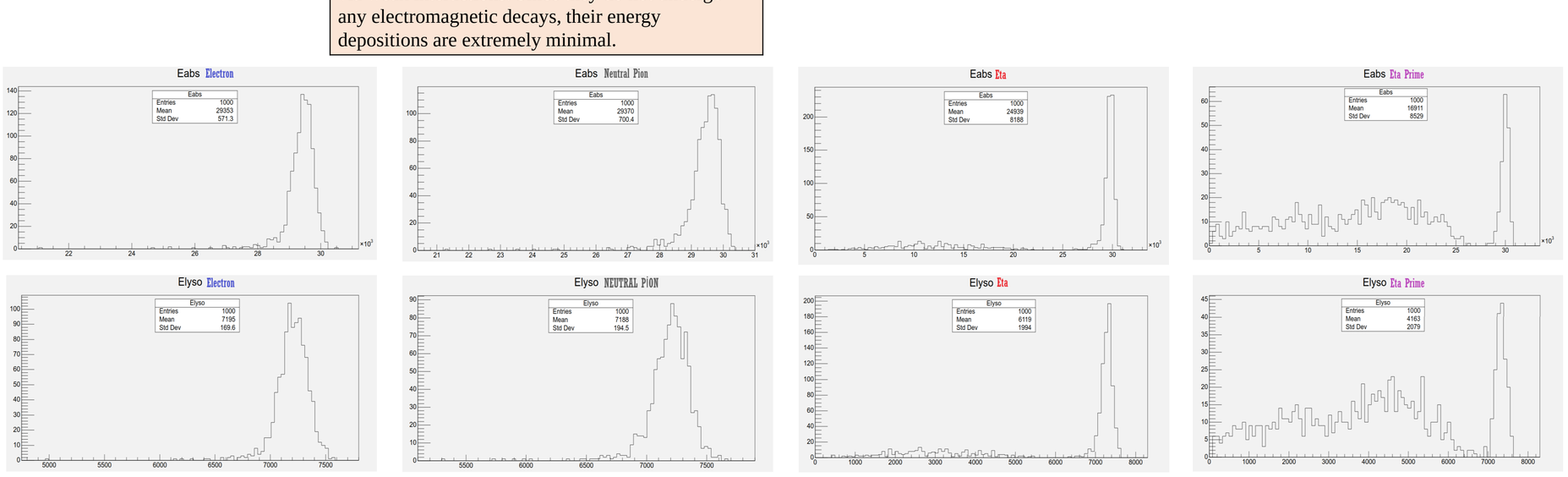

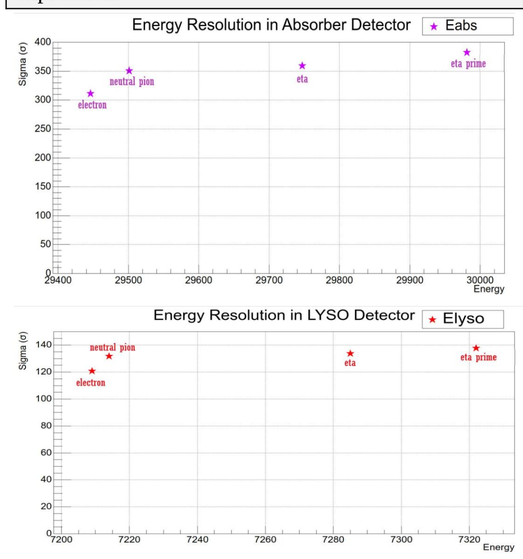

Particle	Depozition Energy	Sigma (σ)	Energy Resolution (σ/E)
e^-	29446	311.9	0.0103
π^0	29501	351.3	0.0118
η	29747	360.0	0.0121
η′	29981	383.0	0.0127

Particle	Depozition Energy	Sigma (σ)	Energy Resolution (σ/E)
e^-	7209	121	0.01670
π^0	7214	132	0.018307
η	7285	134	0.018493
η′	7322	138	0.01884

Energy resolution provides the measure of the energy deposited by a particle onto the detector in the shower max region, which is the maximum energy deposition concentrated in the region without significant energy escape. Among all particles, electrons yield the best results in this regard, as they concentrate their energy in the shower max region. Similarly, the neutral pion exhibited behavior akin to that of the electron. The eta meson, however, started depositing a small amount of energy before reaching the shower max region. For the eta prime meson, it was observed that it deposited a significant amount of energy intermittently as it progressed through the layers.

Conclusion;
This study has contributed to understanding the behavior of different particles with the same energy in the developed RADICAL. It has demonstrated that RADICAL can be utilized not only in high-energy physics but also in fields such as nuclear physics, health physics, and space physics by employing various particles. This is a study that will contribute to the development of calorimeters and detectors across different disciplines.

References

[1] https://www.sciencedirect.com/science/article/pii/S0168900224006636

[2] https://notredame.app.box.com/s/vjpbvpxn2sff72y6y4wvue3nnhcucgtx

[3] https://notredame.app.box.com/s/p9afzt9hxp2yg22vmoycfir8fnnt7tzk

FİZİK BÖLÜMÜ

Solar Power Plant Exploratory Data Analysis and Power Generation Forecasting

Mehmet Karahan Çetinkaya 20022030

Çetin TAŞSEVEN

ABSTRACT

With the increasing global emphasis on renewable energy sources, solar power has emerged as a promising solution to combat climate change and achieve sustainability goals. However, the performance of solar power plants is influenced by factors such as weather conditions, panel orientation, and equipment efficiency, making data analysis and forecasting vital for optimization. This study explores the application of exploratory data analysis (EDA) and machine learning techniques to evaluate and predict the power generation of solar power plants.

Using time-series data from solar plants, including parameters such as irradiation, module temperature, and power output, the study identifies operational anomalies and benchmarks inverter performance. Two machine learning models, Facebook Prophet and XGBoost, are employed to forecast power generation. XGBoost demonstrated superior accuracy with a root mean square error (RMSE) of 504.84 compared to Prophet's RMSE of 1512.75. The analysis also highlights the critical role of irradiation in power generation, supported by the physical principles of photovoltaics.

The findings emphasize the importance of data-driven decision-making in maintaining efficient solar power plants and suggest avenues for future research, including the integration of advanced techniques such as image-based sky view analysis for enhanced forecasting accuracy.

Exploratory Data Analysis

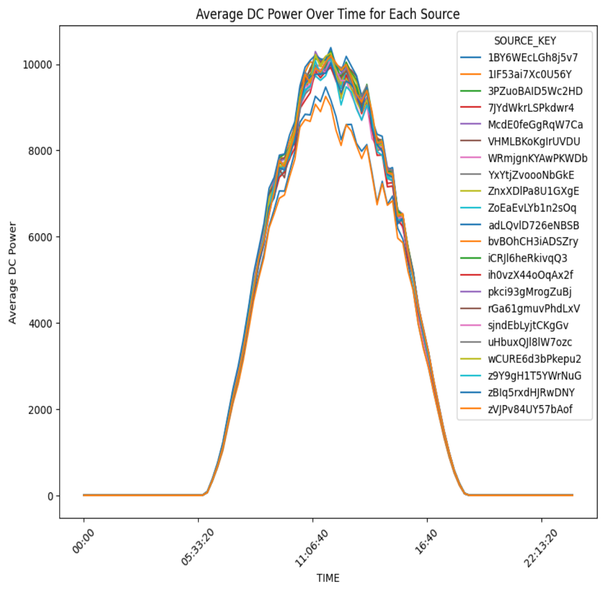

Exploratory data analysis is common step for making a data-driven decison making. The analysis of the merged dataset initially showed no missing or null values, but further investigation revealed that inverters were not equally represented, indicating missing data. The two most frequently entered inverters had the lowest average power generation, which is unusual. Six inverters were identified as having below-average power generation.

Initially, the low performance of the most entered inverter was suspected to be due to either frequent zero values during peak generation times or differing efficiency rates. However, it was later confirmed that all inverters had the same efficiency rate. Further analysis revealed that the poorest-performing inverter had zero values during prime power generation times and some days with missing data, explaining its low average power generation.

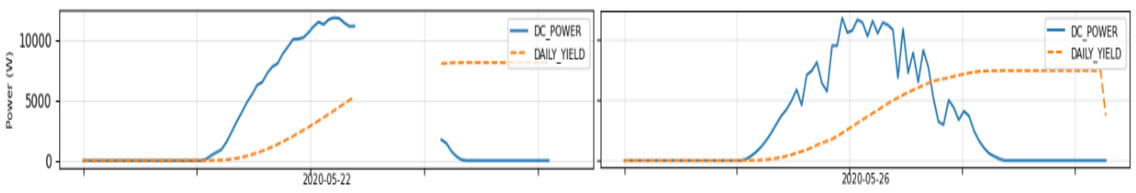

Forecasting

• Feature Selection

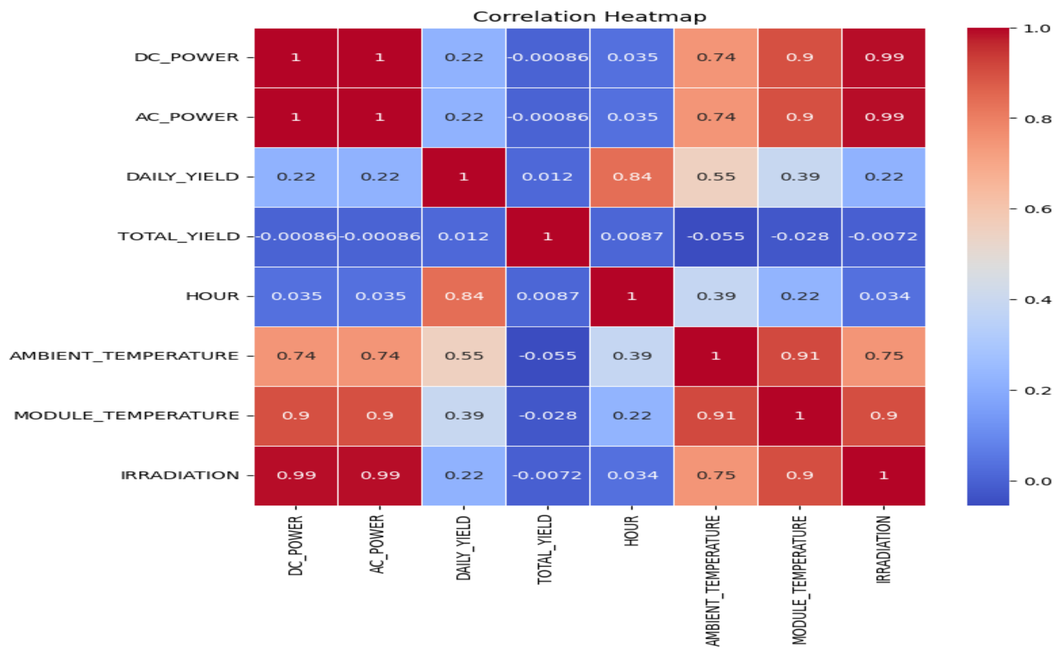

Feature selection is a key step to enhance a model's performance, efficiency, and interpretability. It reduces overfitting on training data, improving the model's generalization, decreases training time, and enhances interpretability by removing unnecessary features. In this study, correlation analysis is used to identify important relationships between features for this purpose.

• Train-Test Split

The first step in building a model is splitting the data into training and test datasets. Typical splits like 80/20 can lead to overfitting in large datasets. To mitigate overfitting, cross-validation methods like TimeSeriesSplit are often used. However, in this study, the short time interval in the data made TimeSeriesSplit unsuitable for trend analysis. As a result, the data was split 80/20 between the train and test datasets.

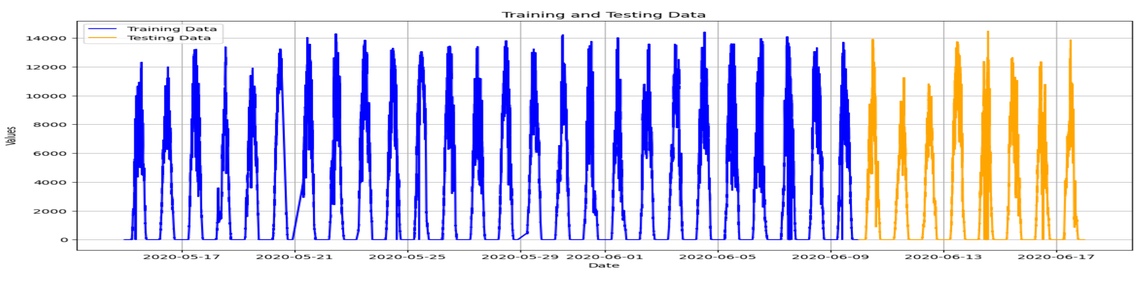

• FB Prophet and XGBoost

After splitting the data into train and test sets, Prophet requires specific column labeling adjustments. The column containing historic data should be renamed to 'ds', and the column with target data should be renamed to 'y'. Then, the model is ready for fitting and prediction. The results and trends of the Prophet model are shown below.

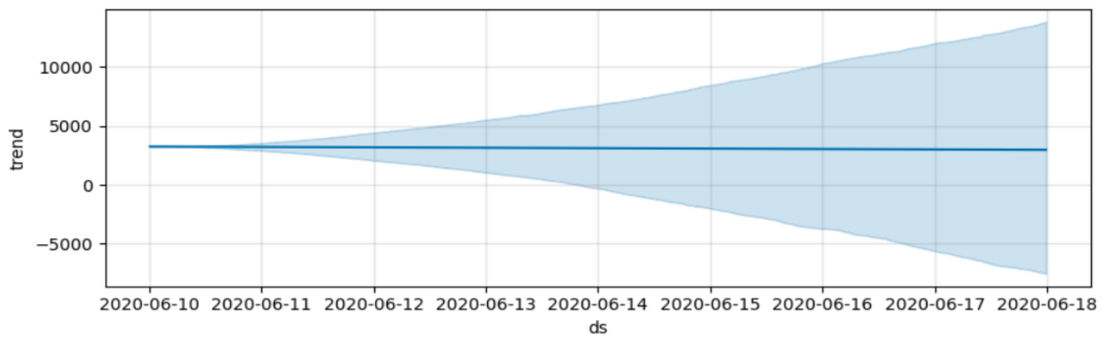

Seeing no change in the trend component is logical because our data is mostly in the same month and we can't expect seasonal changes in the time interval we have in hand.

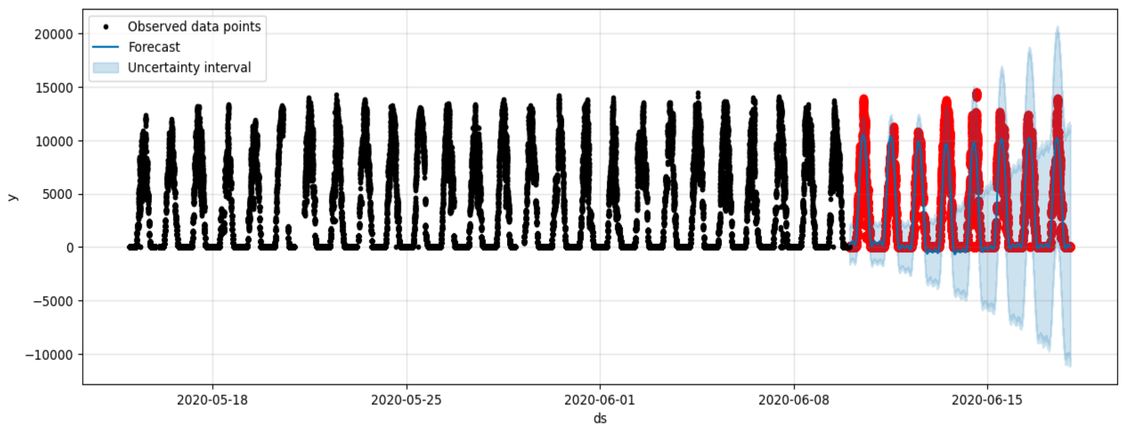

Unlike Prophet, XGBoost does not require a specific data structure. Feature selection is crucial for reducing dimensionality and complexity in the dataset. However, AC_POWER was fully correlated with DC_POWER, and using it could lead to overfitting and data leakage. Similarly, DAILY_YIELD could cause data leakage because it updates after each power generation, potentially revealing future information. Therefore, the selected training features for XGBoost were IRRADIATION, MODULE_TEMPERATURE, AMBIENT_TEMPERATURE, and HOUR. The results of the XGBoost model, along with its graphics, are provided below.

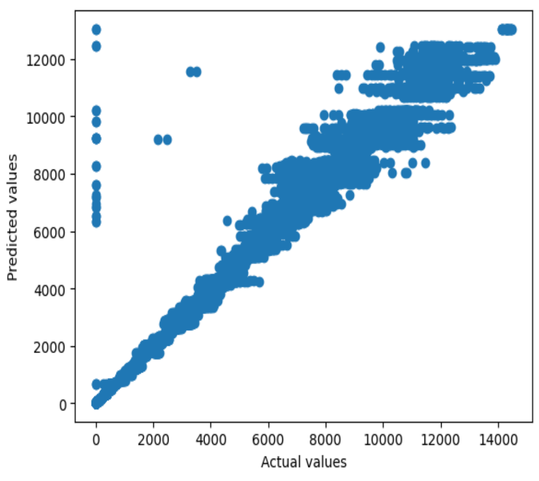

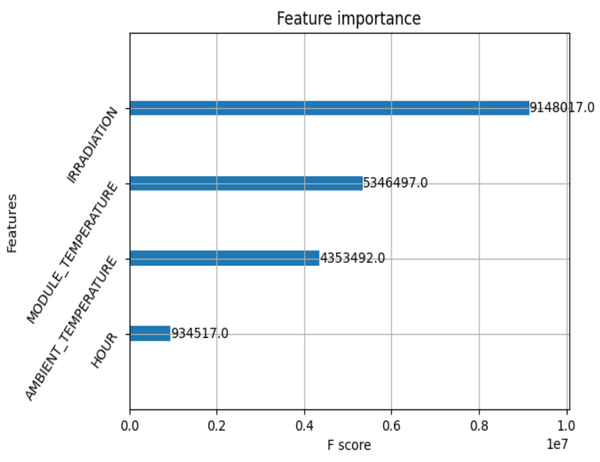

• Conclusion

In conclusion, ensuring a stable and well-maintained power supply requires data-driven decisions and accurate solar power generation predictions. This study outlined data analysis steps and proposed two machine learning models, Prophet and XGBoost, for forecasting. The XGBoost model outperformed Prophet and identified irradiation as the most important feature for solar power generation, aligning with the photoelectric effect's physics. Module temperature also proved significant due to semiconductor properties. Future work could improve the model's performance by incorporating image processing of sky views.

Model	RMSE	MAE
Prophet	1512.75	907.51
XGBoost	504.84	178.91

REFERENCES

[1] Taylor, Sean J., and Benjamin Letham. "Forecasting at Scale." *PeerJ Preprints*,

[2] Simsek, Sinan, Mehmet Isik, and Vedat Gul. "Solar Power Plant Analysis." *Kaggle*

[3] Gupta, Rahul. "Time Series Forecasting of Solar Power Generation Using Facebook Prophet and XGBoost."

Superconductors in Space Missions:

Magnetic Shielding, Radiation Protection and Other Applications

YILDIZ TECHNICAL UNIVERSITY DEPARTMANT OF PHYSICS

Prepared by: Mert Gürlek

Advisor: Prof. Dr. Çiğdem NUHOGLU

ABSTRACT

Active magnetic shielding methods based on the Meissner effect have been thoroughly investigated to address the radiation hazards in space. High-temperature superconductors offer an alternative solution to the high mass and limited protective capacity of passive shielding materials. The effects of active magnetic shielding systems on secondary particle formation have also been evaluated. Hybrid shielding systems, combining passive and active methods, have demonstrated significant success in reducing radiation exposure. Superconducting systems not only protect astronaut health but also present substantial potential for long-term space missions with their energy efficiency and cost-effectiveness.

An Overview of Superconductors and the Meissner Effect

Superconductivity is characterized by the complete disappearance of electrical resistance and the expulsion of an external magnetic field (Meissner effect) once a material is cooled below a certain critical temperature (Tc). This phenomenon was first discovered in 1911 by Heike Kamerlingh Onnes, who observed that mercury, when cooled to 4.2 K, lost all electrical resistance. A microscopic explanation followed in 1957 through the BCS Theory (Bardeen, Cooper, Schrieffer).

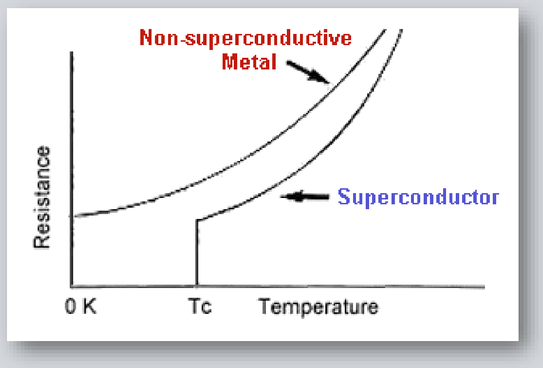

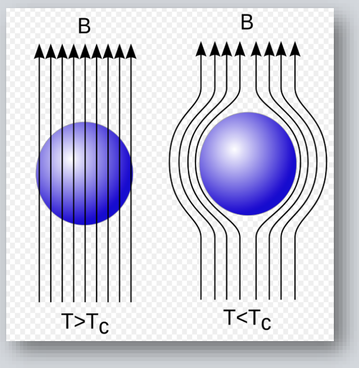

LTS (Low-Temperature) and HTS (High-Temperature) Superconductors

- **LTS:** These materials are typically metallic alloys or pure metals (e.g., NbTi) that operate below 20 K. They are commonly used in applications such as MRI devices and particle accelerators.
- **HTS:** Mostly copper oxide (cuprate)-based ceramics (e.g., $YBa_2Cu_3O_7$) that exhibit superconductivity above 30 K. Because they can be cooled with liquid nitrogen (77 K), they offer advantages for energy transmission and magnetic levitation applications.

Type I and Type II Superconductors

- **Type I:** This category consists of pure metals with a single critical magnetic field (Hc). Exceeding this value completely destroys superconductivity.
- **Type II:** These exhibit a “mixed phase” (vortex structures) between two critical magnetic fields (Hc1–Hc2). Alloys and high-temperature superconductors (e.g., NbTi, YBCO) fall into this group and can maintain superconductivity under higher magnetic fields.

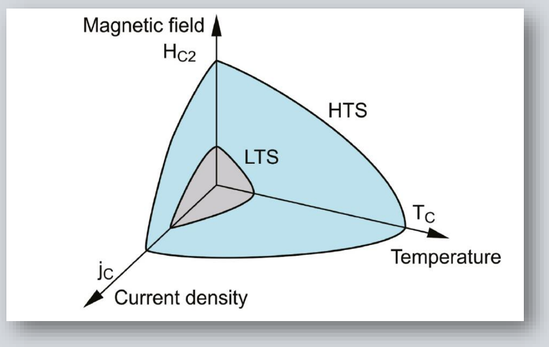

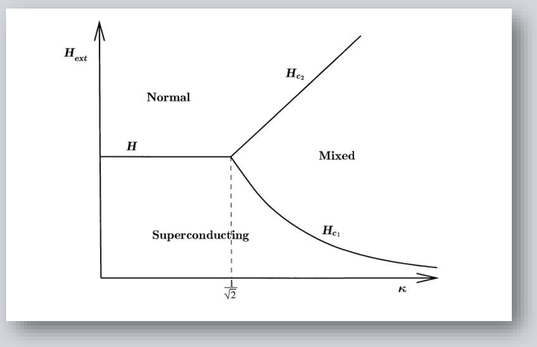

Critical Parameters For Superconductivity

- **Temperature (Tc):** Superconductivity emerges below this temperature; above it, the material reverts to normal conductivity.Critical
- **Magnetic Field (Hc):** The maximum magnetic field strength that a superconductor can withstand without losing its superconducting state (for Type II superconductors, the range is between Hc1 and Hc2).Critical
- **Current Density (Jc):** The maximum current that can flow without disrupting superconductivity. It can be enhanced through microstructural modifications and doping techniques.

The Effects Of Space Envıronment On Superconductors

In space, temperatures dropping to -270°C support low-temperature superconductors (LTS), while high-temperature superconductors (HTS) can operate over a wider range and are more durable. Vacuum conditions prevent oxidation but can cause stress in materials due to gas desorption and temperature fluctuations. In microgravity, cryogenic cooling becomes challenging, although changes in vortex motion can reduce energy losses. Radiation and cosmic rays create defects in superconductors, but materials like MgB_2 can be made more resilient with nano-additives. HTS materials such as YBCO and MgB_2 remain efficient under high magnetic fields, making them ideal for space missions.

Meissner Effect For Spacecraft Magnetic Shielding

The Meissner effect is defined as the expulsion of external magnetic fields when a superconducting material is cooled below its critical temperature (Tc). This property enables the creation of strong, energy-loss-free magnetic fields, which is particularly advantageous in high-radiation environments like space for deflecting charged particles.

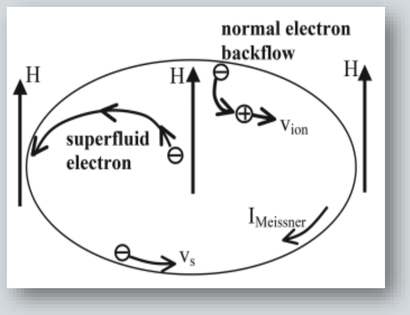

Different Types Of SI Magnetic Development Based On Geometry

- **Toroidal (Torus) Structure:** Provides homogeneous protection in the shielded region while significantly preventing magnetic field leakage; however, it has a mechanically complex design.
- **Solenoid Structure:** Generates a uniform magnetic field along its axis and is suitable for modular designs, but field leakage at the ends may slightly reduce the effectiveness of the shielding.
- **Flat Structure:** The simplest design in terms of production cost and assembly. However, it struggles to generate sufficiently strong magnetic fields in large areas or against high-energy radiation.

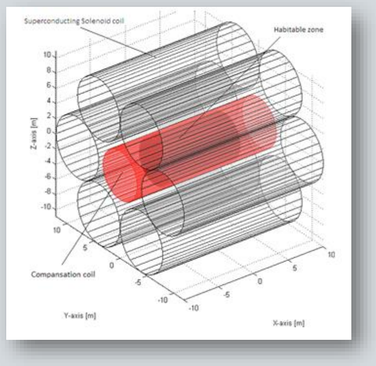

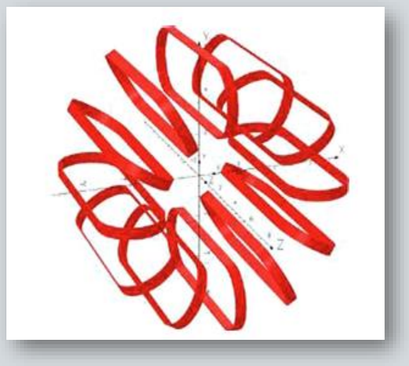

Advantages

- **Energy Efficiency:** Due to zero electrical resistance, they can generate high magnetic fields with low energy consumption, even during long-term missions.
- **Weight Savings**: Creating active magnetic fields instead of relying on heavy passive shielding layers reduces the overall mass of spacecraft.

Disadvantages

- **Cryogenic Cooling Requirement:** The need for superconducting materials to operate at low temperatures increases the complexity of cooling systems and energy demands.
- **Secondary Particle Production:** Interactions with high-energy particles can produce secondary radiation types, such as neutrons and gamma rays, necessitating the use of additional passive shielding layers.

Hybrid Shielding (Passive + Active)

Hybrid systems combine superconducting-based magnetic shielding (active) with low atomic number passive layers. This enhances the magnetic deflection of charged particles while passive layers absorb neutral particles such as neutrons. This approach offers:

- **Mass Savings:** A lighter system design compared to thick standalone passive shielding.
- **Comprehensive Protection:** More effective shielding against both charged and neutral particles and from secondary particles produced by the active shield..
- **Structural Durability:** Thermal expansion differences between superconductors and passive layers pose a long-term challenge that requires careful management.

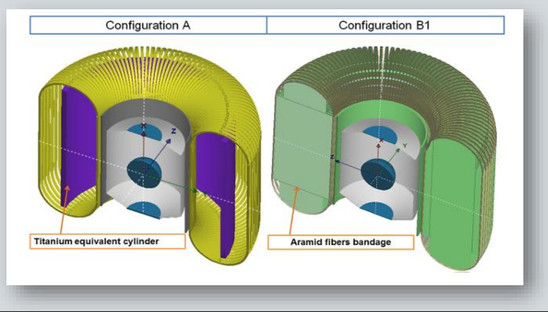

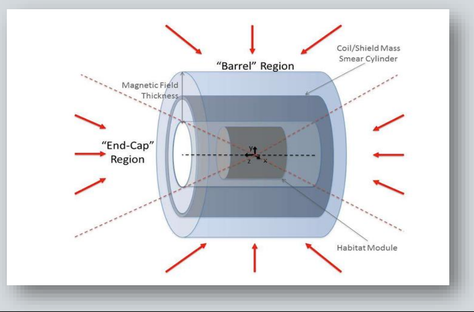

REFERENCES:

[1] **Applications of Superconductivity**
NATO Advanced Study Institute Proceedings, 2000

[2] **Superconductor Theory**
Lecture Notes by Dr. Mohammad A. Rashid, 2019

[3] **Study on superconducting magnetic shield for the manned long-term space voyages**
The Egyptian Journal of Remote Sensing and Space Sciences, 2021

[4] **Monte Carlo simulations for the space radiation superconducting shield project**
Life Sciences in Space Research, 2016

[5] **Magnet architectures and active radiation shielding study (MAARSS)**
NASA Innovative Advanced Concepts Phase II Final Report, 2014

[6] **Evaluation of superconducting magnet shield configurations for long duration manned space missions**
Frontiers in Oncology, 2016

2023-2025 Güz Yarıyılı Fizik BÖLÜMÜ

CONCEPTUAL DESIGN OF ANEUTRONIC FUSION REACTO

Öğrenci Mert TUNA 16022006

Danışman: Prof. Dr. Zeynep GÜVEN ÖZDEMİR

ABSTRACT

A fusion reaction is defined as aneutronic if the total neutron energy from all possible chains is less than 1% of the fusion energy. [1] This type of reaction, if successfully achieved, greatly reduces the problems caused by neutron radiation, including damaging ionizing radiation, neutron activation, reactor maintenance and biological protection, remote operation, and safety requirements. Furthermore, the refueling process is further facilitated by the absence of neutrons as a by-product of nuclear reactions in the system. This enables the construction of reactors with simpler architecture, much more secure, and lower cost.

CONCEPTUAL DESIGN OF ANEUTRONIC FUSION REACTOR

Since Turkey has the world's richest boron reserves, we chose the boron-hydrogen combination for the fuel pair in an aneutronic reaction. The proton-boron fusion reaction. This reaction is an aneutronic reaction and produces three α particles as a product.

$$p + B^{11} \rightarrow 3He^{4} + 8.7\,MeV$$

DESIGN SPECIFICATION

Aspect	Specification	Justification
Complexity	The design should be relatively simple compared to the design of other fusion reactors	Fusion reactors often have complex designs. Simple design is an important requirement for the realisation of the design, reactor construction and maintenance processes.
Material	● The resources to be used should be obtained without any commercial difficulties, and there should be no external dependency in raw materials ● No radioactive waste should be produced	Waste management of the fuel to be used should not be problematic. The reactor should not produce a neutron source. This will simplify the reactor design as well as waste management. In addition, the fuel should be easily available in the target region (Türkiye).
Technological Readiness	The technologies to be used in the construction of the reactor must be available today or have a high degree of technology readiness	The constructability of the reactor with today's technologies will reduce the R&D costs for the reactor and significantly shorten the design, construction and testing time.
Utilization	The reactor should be capable of multiple uses	If the technologies to be used in the reactor can be used in other areas, it will reduce the cost of the reactor and will create gains in different sectors due to the construction of the reactor.

By creating a design specification, we have categorized the processes that will take place in the reactor into classes and prepared an assessment table to obtain the most appropriate results for these processes.

CLASSIFICATION SCHEME

Sub-functions	1	2	3	4
1. Reaction Triggering	Laser	Linear Accelerator (LINAC)	-	-
2. Reaction Stabilization	Inertial Confinement Fusion	Magneto-Inertial Fusion (FRC)	Magneto-Inertial Fusion (Stellarator)	Magneto-Inertial Fusion (Tokamak)
3. Energy Collection	Electrostatic Direct Conversion	Induction Sytems	Travelling Wave Direct Energy Converter	Inverse Cyclotron Converter

ASSESSMENT TABLE

	Complexity	Technological Readiness	Utilization
Variation 1	-	-	-
Variation 2	+	-	-
Variation 3	-	-	-
Variation 4	+	+	-
Variation 5	-	-	+
Variation 6	+	-	+
Variation 7	-	+	+
Variation 8	+	+	+

Although laser fusion is promising, current studies show that systems using linear accelerators give better results.

FRC has no magnetization helicity and has a high β value. The high β makes FRC attractive as a fusion reactor. FRC is well suited for aneutronic fuels because it requires less magnetic field. [2]

Our reactor produces only α particles as products, and the projected maximum efficiency of the Inverted Cyclotron Converter for α particles is 90%. This is in line with the energy converter requirements we expect for our reactor. [3]

Therefore, it is considered appropriate to go through variant 8.

OBJECTIVES TREE

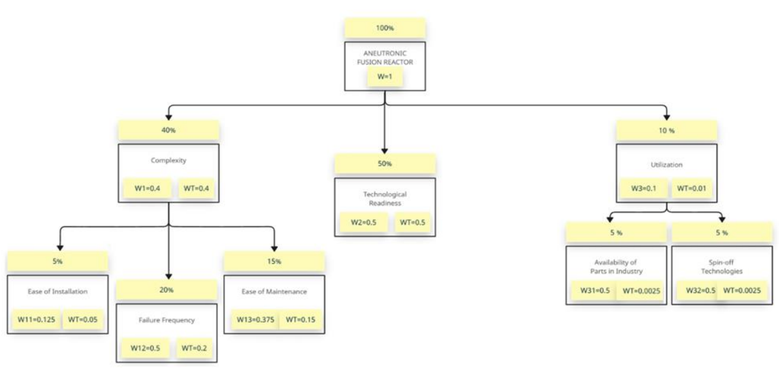

At this stage, we prepared a tree of objectives and assigned a weighting coefficient to each sub-objective.

LAST EVALUATION

	Variant 6				Variant 8			
	W	Variable	Ratio	Result	W	Variable	Ratio	Result
Ease of Installation	0.05	Easy	5	0.25	0.05	Mean	4	0.2
Failure Frequency	0.2	Low	1	0.2	0.2	Low	1	0.2
Ease of Maintenance	0.15	Low	6	0.9	0.15	Mean	3	0.45
Technological Readiness	0.5	High	2	1	0.5	High	6	3
Availability of Parts in Industry	0.05	Low	3	0.15	0.05	Low	2	0,1
Spin-off Technologies	0.05	Less	2	0.1	0.05	More	5	0.25
W_{Total}				W_T=2.6				W_T=4.2

We revalidated the results according to the parameters we set in the objectives tree. The variant 6 that we have compared is laser-based, and variant 8 is based on the linear accelerator that we chose in the previous point. We did not re-compare variant 4, which might be more technologically ready than variant 6, as the energy recovery method is not attractive.

VALUE PROFILE DIAGRAM

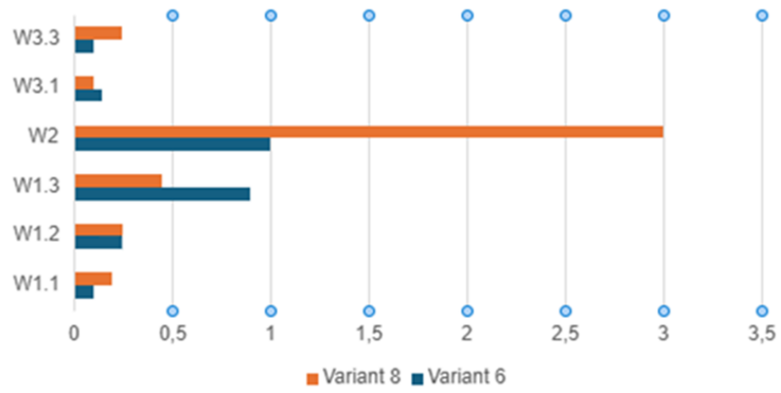

RESULT

Our result is in line with the studies conducted by TAE Technologies. Based on this system, the company is also working in medical fields such as Boron Neutron Capture Therapy, which uses similar subcomponents (e.g., accelerators). As a result of our study, we share a representative image of a reactor developed by the company.

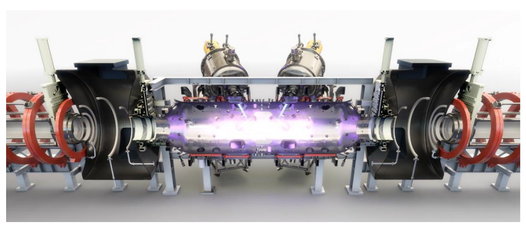

Figure TAE Technologies C-2W (a.k.a. Norman) reactor chamber

KAYNAKÇA

[1] Kikuchi, M., Lackner, K., & Tran, M. Q. (Eds.). (2012). Fusion Physics. International Atomic Energy Agency. Vienna.
[2] E. Kawamori, Y. Murata, K. Umeda, D. Hirota, T. Ogawa, T. Sumikawa, T. Iwama, K. Ishii, T. Kado, T. Itagaki (2005), Ion kinetic effect on bifurcated relaxation to a field-reversed configuration in TS-4 CT experiment, Nuclear Fusion, 45, 843
[3]] Monkhorst, Hendrik J. & Rostoker, Norman, "Controlled fusion in a field reversed configuration and direct energy conversion", US patent 6850011, issued 2005-02-01

FACULTY OF ART AND SCIENCE

2024-2025 Fall Semester DEPARTMENT OF PHYSICS

Ammonia Sensing Performance of ZnO Nanostructures Fabricated by Varied Morphologies

Batuhan KALAFAT 19022011

Supervisor: Prof. Dr. Zeynep GÜVEN ÖZDEMİR

ABSTRACT

In this study, structural, morphological and optical characterizations of ZnO nanostructures obtained by sol-gel and hydrothermal methods were performed and their ammonia (NH3) sensing performances were compared.

Fabrication of ZnO Nanostructures

Fabrication of Thin Film by Sol-Gel Method

0.25 M $Zn(CH_3CO_2)_2$-$2H_2O$ salt was prepared by stirring in 10 mL 2-methoxyetanol for 24 hours in a magnetic stirrer.

Fabrication of Nanoparticle by Hydrothermal Method

While 0.25 M $Zn(CH_3CO_2)_2$-$2H_2O$ salt is dissolved in methanol, 0.3 g KOH is dissolved in methanol in a separate container and these two solutions are mixed slowly. This solution, which was thrown into the autoclave, was left in the oven at 180°C for 12 hours and the particles formed were washed first with pure water and then with methanol. It was dried at 80°C for 4 hours.

Sensing Experiments of the Sensors to Volatile Organic Vapor

In its simplest form, a gas sensor consists of a sensing unit and a "transducer" element responsible for converting the changes in some physical properties of the sensing unit as a result of the interaction of the sensing unit with target molecules (ammonia in this study) into an easily measurable electrical and/or optical signal. In this study, Au electrode structure with 50 µm spacing on Plexiglas will be used as the "transducer" in ZnO-based gas sensors. The working principle of the sensor will be based on measuring the changes in the electrical conductivity of the sensing unit (ZnO nanostructures). In this context, ZnOs prepared with sol-gel and prepared as particles were coated by spin coating method at 3000 rpm for 30 seconds. The films coated on IDT were annealed at 200 °C for 12 hours and the sensing tests were measured with the setup in Figure 1.

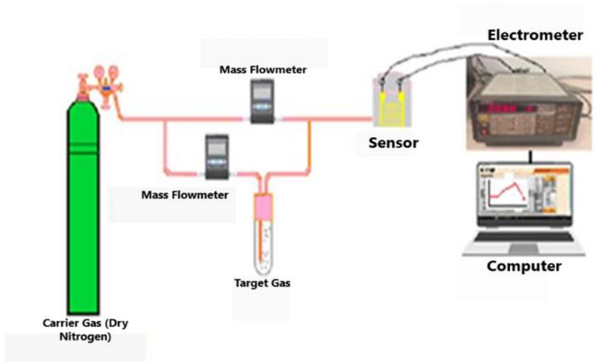

Figure 1 Experimental Setup for Sensing Experiments

RESULTS

Structural and Morphological Characterization of ZnO Nanostructures

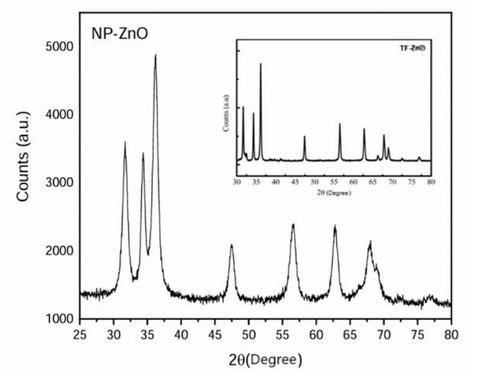

Figure 2 XRD Spectra of ZnO Nanostructures

XRD spectra of sol-gel grown thin film ZnO (TF-ZnO) and NP-ZnO (NP-ZnO) films grown from particles formed by HT are as shown in Figure-2. In the XRD spectrum obtained for ZnO, the observed purity of 2θ at 31.67°, 34.33°, 36.15°, 47,46°, 56.52°, 62.78°, 66.29°, 67.88°, 69.02°, 72.47° ve 76.88° The peaks observed at □ are reflections in the crystal planes (100), (002), (101), (102), (110), (103), (200), (112), (201), (004), and (202), respectively (JCPDS Card No. 01-79-0207).

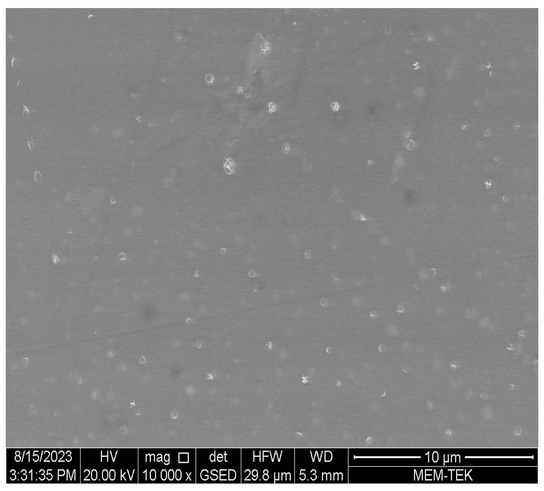

Figure 3 SEM Images of ZnO Thin Film

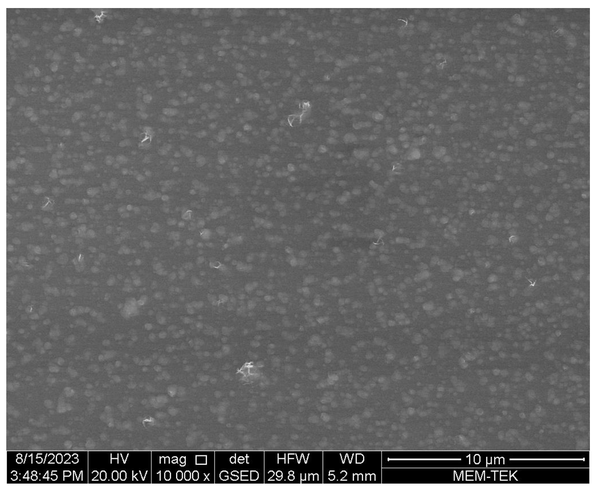

Figure 4 SEM Images of ZnO Nanoparticle

SEM images were obtained under 10 000 magnification with a scale of 10 micrometers corresponding to 200 nm. As can be seen from Figures 3 and 4, it is observed that the ZnO film is quite homogeneous and nano-sized.

Optical Characterization of ZnO Nanostructures

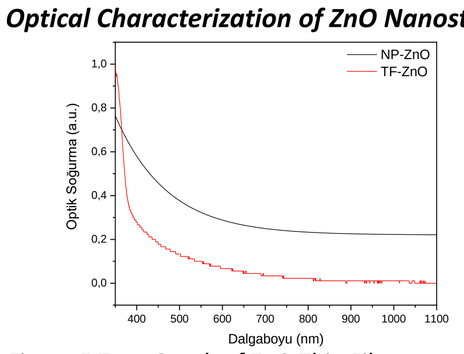

Figure 5 Tauc Graph of ZnO Thin Film

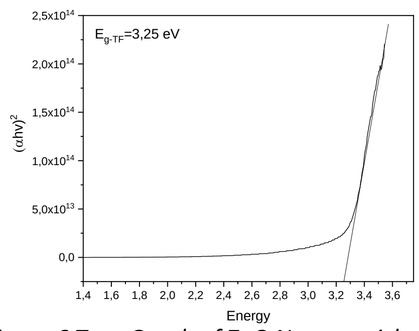

Figure 6 Tauc Graph of ZnO Nanoparticle

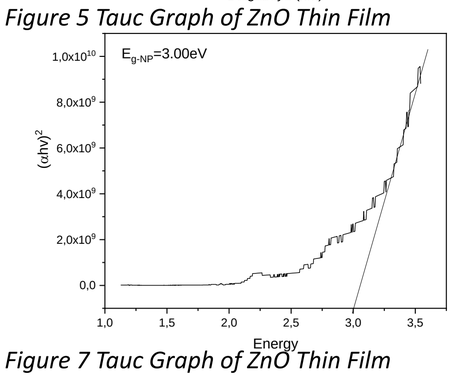

Figure 7 Tauc Graph of ZnO Thin Film

The optical properties of ZnO thin films were characterized by measuring the absorption coefficients by UV-vis spectrometry in the wavelength range of 350-1100 nm (Figure 5) From the measured absorption coefficients $(\alpha h\nu)^2 = A(h\nu - E_g)$ Optical band gaps were calculated with the help of the relation. The band gap for TF-ZnO was calculated as 3.25eV (Figure 6), while the band gap for NP-ZnO was calculated as 3.00 eV (Figure 7).

Detection Results for ZnO Nanostructures

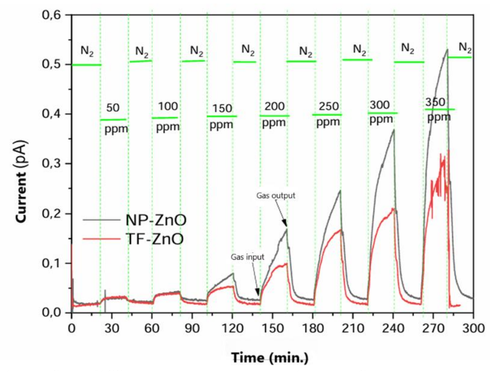

Figure 8 Sensor current with time for different concentrations of ammonia vapor at room temperature

The room temperature ammonia sensing performance of ZnO-based sensors fabricated by sol-gel and hydrothermal method is shown in Figure 8. Sensor tests were performed at ammonia concentrations ranging from 50 ppm to 350 ppm. It is seen that the sensor responses increase with increasing ammonia concentration. It is clear that the sensor response produced using ZnO nanoparticles synthesized by hydrothermal method responds better to ammonia gas. This can be attributed to the increase in adsorption sites due to the increase in the surface area/volume ratio at the nanoscale. The sensing properties are related to the crystal phase, nanostructure and particle size of the sensing material. [1,2,3]

Sensing Mechanism of ZnO

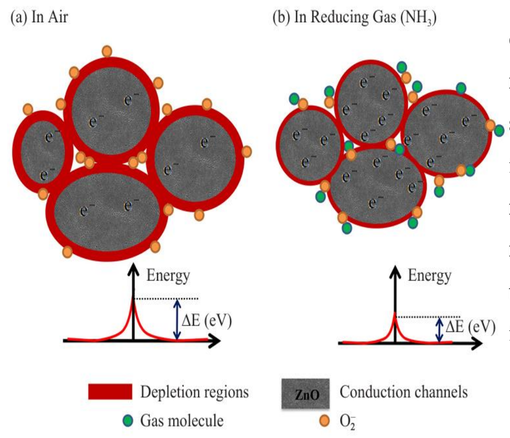

ZnO is a typical chemoresistive gas sensing material. Gas sensing occurs when the target gas interacts with the sensor surface. This phenomenon, called adsorption, is when the target gas combines with oxygen molecules on the sensor surface, causing an electrical change. The ZnO surface adsorbs oxygen molecules in the atmosphere and these molecules form negatively charged oxygen ions on the surface. Ammonia is a reducing gas and chemically interacts with the ZnO surface. Ammonia molecules ($\boldsymbol{NH_3}$) react with adsorbed oxygen ions on the surface. During this reaction, oxygen ions combine with $\boldsymbol{NH_3}$, resulting in the release of free electrons from the surface.

$$\boldsymbol{O_2(gas) + 2e^- \rightarrow 2O^-}$$

$$\boldsymbol{NH_3 + 3O^- \rightarrow N_2 + 3H_2O + 3e^-}$$

ACKNOWLEDGEMENTS

I am profoundly grateful to my esteemed instructor, Researcher Ayşe Nur ŞAHİN, whose invaluable guidance, expertise, and unwavering support were instrumental throughout the preparation phase of my experimental studies. Her exceptional knowledge, patient mentorship, and thoughtful encouragement have not only enriched my academic journey but also inspired me to strive for excellence. I feel truly fortunate to have had the opportunity to learn from such a dedicated and insightful educator, and I will always cherish the impact she has had on both my studies and personal growth.

REFERENCES

[1] K.Shingange.., Highly selective NH3 gas sensor based on Au loaded ZnO nanostructures prepared using microwave-assisted method, Journal of Colloid and Interface Science 479 (2016) 127-138

[2] C.Li…, NH3 sensing properties of ZnO thin films prepared via sol–gel method, Journal of Alloys and Compounds 606 (2014) 27–31

[3] J.-H. Lee, Gas sensors using hierarchical and hollow oxide nanostructures: overview, Sensors Actuators B Chem. 140 (2009) 319–336